Atomization Based Dual Regime Spray Coating System: Design and Applications

by

Maxym Rukosuyev
Specialist, Simferopol State University (Ukraine), 1997
BEng, University of Victoria, 2012

A Dissertation Submitted in Partial Fulfillment
of the Requirements for the Degree of

DOCTOR OF PHILOSOPHY

in the Department of Mechanical Engineering

Supervisory Committee

Atomization Based Dual Regime Spray Coating System: Design and Applications

by

Maxym Rukosuyev
Specialist, Simferopol State University (Ukraine), 1997
BEng, University of Victoria, 2012

Supervisory Committee

Dr. Martin Byung-Guk Jun, Department of Mechanical Engineering
Supervisor

Dr. Colin Bradley, Department of Mechanical Engineering
Co-Supervisor

Dr. Zuomin Dong, Department of Mechanical Engineering
Departmental Member

Dr. Alexandre G. Brolo, Department of Chemistry
Outside Member

Dissertation Summary

Supervisory Committee

Dr. Martin Byung-Guk Jun, Department of Mechanical Engineering

Supervisor

Dr. Colin Bradley, Department of Mechanical Engineering

Co-Supervisor

Dr. Zuomin Dong, Department of Mechanical Engineering

Departmental Member

Dr. Alexandre G. Brolo, Department of Chemistry

Outside Member

In modern research and industrial applications, the importance of coatings can hardly be underestimated. Coatings are used extensively in optics, biomedical instruments, cutting tools, and solar panels to name a few. The primary purpose of any coating is to alter surface properties of the base material thus adding new functionality or improving the performance of the original product. A multitude of coating techniques has evolved over the years with spray coating being one of the more widely used. Some applications require deposition of materials that are either in the form of a solution or suspension. Therefore, before or during the deposition process small droplets of the said liquid are formed and transferred onto the substrate. Since differently sized droplets have different surface impact dynamics, droplet velocity at the impact plays an important role in the way it will adhere to the surface. Most spray coating techniques do not take into account the process of droplet-surface interaction which may result in overspray, poor coating thickness control, and material waste.

The research presented in this dissertation outlines the supporting principles, design, fabrication and testing of an innovative spray coating system that provides the ability to fine tune coating parameters, including droplet impact velocities, to provide close to optimum deposition conditions. The core of the design consist of a dual velocity nozzle unit that ensures acceptable range of droplet velocities at the surface, while keeping droplets from accelerating excessively inside the system. Early experiments showed the system's potential to produce nanoparticle coatings with particles uniformly distributed across the substrate. In addition, pigment coating for improved 3D scanning was also performed, thereby improving the surface definition and accuracy of the scanning results. Scalability of the system also led to experiments in applying this technology to microprinting. Preliminary microprinting results illustrated the system's flexibility and opened new research avenues in micro-coating, microprinting, and, possibly rapid prototyping. Furthermore, thanks to the highly adaptable nature of the proposed design, seamless incorporation of a torch-like device into the nozzle unit was also possible. That provided the opportunity to perform *in situ* thermal processing or sintering of deposited material as well as production of a nanoparticle coating in a one-step process by thermally decomposing precursor solution.

Technology developed during the research work presented in this dissertation demonstrated its ability to be adapted in a number of applications that can benefit both industry and engineering research alike. Large area coatings, nanoparticle production, micro-coating, and coatings for improved 3D scanning are just a few areas where the presented technique can already, or may, if developed further, outperform existing and

widely accepted methods. Fine tuning of the system to a particular application, and tapping into its potential in other fields will be explored in future research.

Table of Contents

List of Tables

List of Figures

List of symbols

D_m	Mean droplet diameter.
T	Liquid surface tension.
f_a	Ultrasonic atomiser piezo crystal resonant frequency .
We	Weber number (dimensionless). Signifies relative importance of fluid inertia compared to surface tension (capillary forces).
w_0	Droplet velocity normal to the surface.
ρ	liquid density.
Oh	Ohnesorge number (dimensionless). Relates viscous forces to inertial and surface tension forces.
K_m	Dimensionless number that binds together Weber number and Ohnesorge number in order to mark the cut-off condition for splashing regime upon droplet impact onto hard surface.
K_{mc}	Critical K_m. For $K_m > K_{mc}$, droplet will enter splashing regime.

ACKNOWLEDGEMENTS

I would like express my gratitude for help and continuous support of my supervisors Dr. Martin Jun and Dr. Colin Bradley during the time of my graduate studies. Their thoughtful guidance and advice helped me to successfully complete my work and hone my skills as an engineer.

Also, I would like to acknowledge financial support from Natural Sciences and Engineering Research Council of Canada (NSERC), Korea Institute of Machinery and Materials (KIMM), and University of Victoria during the course of PhD program.

Last, but by no means least, I would like to thank my wife and best friend Olga for her love, support, understanding, and encouragement throughout the course of my engineering degree program.

Chapter 1 **Introduction**

In modern research and industrial applications, the importance of coatings can be hardly underestimated. Coatings are used extensively in optics, biomedical applications, cutting tools, and solar panels to name a few [1-6]. The primary purpose of any coating is to alter the surface properties of the base material thus adding new functionality or improving the performance of original part.

A plethora of coating methods has been developed over the years. Material deposition methods such as dip coating or spin coating [7-10] can provide adequate results in some applications where coating thickness does not play a significant role. Spin coating can be successfully used on smaller samples in cases of coating material being high viscosity liquid which does not easily lend itself for other coting methods. Dip coating can be used for large area coating in cases when coated material can be rolled into long sheets, but is difficult for larger sized samples of rigid materials. It also requires large coating facilities with significant fluid volumes. Methods such as chemical of physical vapour deposition [11-13] provide great results with outstanding thickness control (capable of depositing atomic layers of material). However, the use of these methods is limited by the necessity of having to perform the coating process in vacuum. Therefore, the areas that can be coated are usually quite small. In addition, these methods require the use of highly specialized and expensive equipment. Electroplating and anodizing are two methods that have been used extensively for metal coating [14-18]. Their use however, is limited by the properties of the substrate i.e. it should be conductive, or made conductive by prior coating in conductive materials. Plasma coating [19-21] can be successfully used on metal substrates that can withstand higher temperatures. It provides great adhesion to the

base material but layer thickness control and thermal load exerted on the substrate during the coating process limit its use. All of the coating methods described above have their merits in particular industrial or research applications. There is, however, no such thing as a universal coating technique that can be used with any material on any substrate. Further review of coating methods relevant to the research presented in this dissertation can be found in each respective chapter.

Spray coating is one of the more widely used methods of depositing materials. Most spray coating techniques however, do not take into account the process of droplet-surface interaction which may result in overspray, poor coating thickness control, and material waste. Research presented in this dissertation is aimed at developing an efficient and cost effective novel spray coating technique which incorporates droplet velocity control based on droplet size. Furthermore, testing the system in real world engineering applications formed another part of the research.

The basic idea to apply droplet dynamics control to coating processes stemmed from the previous research in the use of spray coolant/lubricant for milling application [22] and the later study of its effects in micro-milling [23, 24]. Specific requirements for the coolant/lubricant application in micro-milling led to the concept of cutting zone penetration in order to provide appropriate temperature and lubricity control during the cutting process. Since flood cooling is next to impossible in micro-milling due to the very high rotational speed of the tool (which creates cavitation and prevents efficient cooling of the cutting zone), forced spray cooling was proposed as a novel approach to cooling in micro-machining. To ensure efficient cutting zone penetration and spreading of the coolant droplets, the spray should be delivered with velocities that fall in a certain range.

Early experiments in micro-milling cooling systems produced basic concepts that later were used in the coating system development. However, this technology could not be directly applied for spray coating. Nozzles with special geometry had to be developed to effectively deliver atomized droplets of material to the coated surface.

The novelty of the presented work is primarily found in the development of the coating nozzles that create a dual velocity regime inside the coating nozzle. As a result of droplets having different velocities inside and outside of the nozzle, condensation inside the nozzle can be avoided whereas the spreading of the droplet on the coated surface is ensured. Furthermore, once applied onto the surface, many nanoparticle coatings require post curing or sintering to provide better adhesion and/or remove polymer nanoparticle encapsulation [25]. Furthermore, some coatings use pyrolysis to facilitate the formation of nanoparticles from a precursor solution [26]. However, injection of the particles into the flame from the side produces uneven heating of the particle stream which leads to lower deposition rates, more waste, and reduced coating quality. Using concentric geometry intrinsic to the proposed nozzle design, a thermal spray treatment setup could be seamlessly incorporated into the device. Therefore, the resulting coating system can be used both in “cold” (for room temperature coating), and in “hot” (when elevated temperatures are required) mode of operation. “Hot” operational conditions provide the means to either sinter/heat-treat particles already contained within spray droplets, or generate new particles using pyrolysis of the precursor solution. The latter can be used either for nanoparticle production or as a one-step coating process that eliminates the need for a costly separate particle production stage.

The technology presented in this research forms a basis for further development of the dual velocity coating system. Further tailoring of this technique to a particular application's requirements is needed to achieve optimum results. Some examples of the system's capabilities in optical coatings, hydrophilic coatings, nanoparticle generation, and coating for 3D scanning are presented in later chapters of this dissertation.

1.1 Dissertation outline

This dissertation consists of four papers that have already been published, submitted for publication to a peer-reviewed academic journal, and/or presented at international conference. Information on each publication is located at the beginning of each chapter.

Chapter 2 discusses the need for the development of a novel coating device that is able to overcome the shortcomings of the coating systems that are presently available. Furthermore, the chapter outlines the theory behind droplet impact dynamics, which serves as a foundation for the design of the device, and the fluid flow parameters that have to be achieved in order to produce desired coating results. Next, the design idea of a dual velocity coating system with a separate ultrasonic atomization unit is introduced and its functionality explained. Chapter 2 concludes with the preliminary evaluation of coating results obtained by using the system. Such applications as microprinting, antireflective coating on glass surfaces, and coatings for improved 3D scanning are also explored and relevant coating results are presented at the end of the chapter.

Chapter 3 focuses on the application of the technology described in Chapter 2 for applying antireflective and antifogging silver nano-particle coatings onto a glass substrate. Silver is used extensively in medical applications for its antimicrobial/antibacterial properties. In addition, silver particles are utilized in coating of photovoltaic panels to

reduce fouling and increase efficiency. The combination of material properties, particle size and uniform application of the nanoparticles produces a superhydrophilic surface, which in its extreme also has antifogging properties. The antifogging effect is created when the liquid contact angle on the surface is reduced rapidly thereby eliminating light scattering off of the individual droplet surfaces. The antireflective properties of the obtained coating can also be combined with the antibacterial effect found on optical devices to produce surfaces that provide less grip for bacteria or mold, thus having antifouling properties.

Chapter 4 is a continuation of the previous chapter as the experiments are carried out using the same silver nanoparticles as coating material. The coating method however, is altered by adding a torch-like device which facilitates in situ thermal treatment of nanoparticles. Heating nanoparticles can serve several functions such as rapid solvent evaporation, disposing of an encapsulating polymer left after particle production, sintering, and simultaneous heating of the substrate for better adhesion. The ability of the system to effectively process nanoparticles at elevated temperatures and deposit them onto the substrate surface was successfully demonstrated.

Chapter 5 describes the use of the system for a one-step coating process that includes production of the nanoparticles and their subsequent deposition onto the substrate. Using the same approach as in the previous chapter of creating a “hot” region on the droplet’s path of travel, a solution of silver nitrate is instead of silver nanoparticle suspension. At elevated temperatures, silver nitrate decomposes producing silver nanoparticles as a result of the pyrolysis process. As the droplet travels through the flame, silver particles are formed and deposited onto the substrate. This process eliminates the need for an

additional step of particle production and can be used with other precursor solutions to produce coatings with different functionality.

1.2 Research contributions

Research presented in this dissertation represents a gradual development of the idea of coating velocity control. Room temperature operation optimization was the first milestone that was reached with the development of the dual regime coating system. Further "probing" of the system's potential, revealed its great adaptability and ease of modification to expand its functionality. Downscaling of the system led to early experiments in micro-printing. Furthermore, the addition of the heat treatment arrangement allowed utilization of system's added functionality by potentially eliminating or significantly reducing post-curing of the resultant nanoparticle coating. Flame spray pyrolysis technique developed using annular flame design moved the efficiency of the system yet further by allowing the *in situ* synthesis of nanoparticles for simultaneous coating or collection for further processing.

The novel contributions that result from this research work and are presented in this dissertation are summarized below:

i) **Development of a novel coating device:** A coating device that uses dual velocity nozzle is designed developed and initially tested. The nozzle creates low velocity flow internally to prevent condensation and formation of larger droplets while providing close to optimum velocity at the surface. The nozzle provides the means to conduct additional sorting of droplets by size, which creates a more consistent coating and results with minimal or no overspray or wasted material. Thanks to its intrinsic scalability, the system can be easily adapted to large area

coatings as well as to micro-printing with only minor design modifications. Since the droplets are produced separately from the deposition unit, the user can utilize several droplet sources with various materials and mix them just prior to deposition allowing for production of composite coatings (see Chapter 2). This work was published in the Journal of Coatings Technology and Research [27].

ii) **Antifogging/superhydrophilic and antireflective silver nanoparticle coating:** As the coating system introduced in Chapter 2 was capable of producing sub-micron thickness coated layers, silver nanoparticles synthesized "in house" were used to create functional glass coatings. As a result, fine, nanometer scale structure was created on the surface that exhibited strong superhydrophilic behaviour and produced antifogging effect. In addition, the ability of the resultant coating to increase light transmission in the visible spectrum was also discovered. That unique combination, together with silver's antibacterial properties, creates a coating that can potentially be attractive in several industrial and research applications for biomedical devices, optics, photovoltaic panels, etc. (see Chapter 3). This paper was published Journal of Coatings Technology and Research [28].

iii) **Thermally assisted silver nanoparticle coating:** Based on the same general nozzle design introduced in Chapter 2, a new feature was added to facilitate in-process thermal treatment of the droplets/particles. Since the material used for experiments is similar, resulting coating exhibits properties like those seen in Chapter 3. However, the use of a built in torch-like device enables removal of any polymer remaining on the surface of particles after they have been produced. Due to its unique concentric design, the nozzle introduced in this chapter will produce

a “hot” region that has a dome-like shape and is completely axisymmetrical with the droplet jet. This unique feature eliminates the negative effect of thermophoresis that can induce particle migration along the thermal gradient direction from “hot” to “cold” regions. Therefore, more droplets/particles are heated evenly thus undergoing the same thermal treatment producing more consistent coating results (see Chapter 4). This paper was presented at the 11th International Conference on Micro Manufacturing (ICOMM 2016) and published in ASME Journal of Micro- and Nano-Manufacturing [29].

iv) **Novel one-step coating process with *in situ* silver nanoparticles synthesis:** The research presented in Chapter 4 builds on the previous chapter and extends the concept of the thermal treatment of atomized droplets. As opposed to the experiments described in Chapter 3, elevated temperature at the exit of the nozzle in this case facilitate pyrolysis process. Droplets of the precursor solution, while passing through the “hot” portion of the nozzle, are heated to the level where thermal decomposition of the precursor can occur. Nanoparticles are formed as a result of this chemical reaction. Factors like the size of a droplet, travel time of the droplet through flame, precursor concentration, and maximum flame temperature play an important role in the formation of particles. The system presented in this paper allows for tuning of the parameters to achieve desirable particle characteristics as well as simultaneous deposition of formed nanoparticles onto a substrate (see Chapter 5). This paper was presented at the World Congress on Micro and Nano Manufacturing (WCMNM 2017) and its extended version (in

this dissertation) is submitted for publication to the Journal of Coatings Technology and Research.

Chapter 2 **Design and application of nanoparticle coating system with decoupled spray generation and deposition control**

This paper was published in Journal of Coatings Technology and Research in 2016. Maxym Rukosuyev, Oleksandr Barannyk, Peter Oshkai, and Martin Jun.” Design and application of nanoparticle coating system with decoupled spray generation and deposition control”, Journal of Coatings Technology and Research, 13(5) (2016), pp. 769-779.

This chapter introduces problems faced by the spray coating in general and outlines possible solutions. Operating principles, design, and parameters tuning for the novel spray coating technique are described and evaluated. In addition, a series of experiments illustrating system’s ability to deliver cost effective solution in various coating applications is also presented.

Contributors:

Maxym Rukosuyev – designed, manufactured, tested the coating system, and completed the manuscript.

Oleksandr Barannyk – aided in the setup and data processing during the PIV analysis, and compiling the corresponding section of the manuscript.

ABSTRACT

Coatings are widely used in various applications to change the interaction of the surfaces with external media. The key factors that determine the quality of a spray-coated layer are the size (order of a few microns in diameter) and dimensional uniformity of droplets in the spray and the droplet impact velocity. For many applications, coating quality is strongly dependant on the method and equipment used during the application process. This paper presents development of a decoupled system for spray coating and micro printing, which includes an ultrasonic spray generation device and a nozzle for the spray deposition independently operated. Design and development of the system as well

as testing for different applications are presented in this paper. The system design can be potentially used for large area coating, such as windows and solar panels, as well as micro printing of electronic circuits and numerous other applications.

2.1 Introduction

The range of applications requiring various types of coatings stretches from biomedical devices to microelectronics, and the number of technological solutions provided by the use of advanced coating materials is still growing. Coatings are used extensively to enhance the surface properties of different substrates. Such properties include abrasion resistant [6] and antireflective coatings[5, 30] on glass surfaces in various devices or wear resistant coatings[1] on friction surfaces of various mechanical components. In addition, conductive, light sensitive, and conformal coatings are frequently used in the construction of printed microelectronic devices and photovoltaic panels [4, 31]. Coatings are widely used in various biomedical applications to change the interaction of the surfaces with bioactive materials[2]. Two characteristics of the coatings that are of primary importance are the coating uniformity and coating thickness control. The key factors that determine the quality of a spray-coated layer are the size (order of a few microns in diameter) and dimensional uniformity of droplets in the spray and the droplet impact velocity[32]. For many applications, coating quality is strongly dependant on the method and equipment used during the application process.

Quite often, to produce a functional coating, suspensions of various nanoparticles are used. In that case, atomised droplets will contain nanoparticles within, which will be left on the coated surface once the liquid solvent is evaporated. The need for small size of the

atomized droplets arises from the fact that in order for the nanoparticle coating to be uniform across the surface, one would require the particles to be finely dispersed within an atomised droplet. In the case of larger droplets, nanoparticles inside the liquid tend to agglomerate[33]. Therefore, once deposited, nanoparticle agglomerates are left on the surface thus increasing surfaces' roughness and decreasing the coating's uniformity. Consequently, the fewer nanoparticles are in a single droplet, the more uniformly they will be distributed over the coated surface and the better the coating thickness control will be.

Traditionally, conventional air pressure atomising nozzles are used for spray coating [34-36]. Although providing adequate performance in most spray coating applications, drawbacks associated with this method make it unsuitable when tight thickness and uniformity requirements are in place. Due to the nature of the atomisation mechanism in air atomising nozzles, one should have certain air pressure to ensure atomisation. That limits the range of spray velocities that can be controlled. In addition, droplet size distribution is non-uniform, strongly dependant on the pressure applied, and generally in the region of tens to hundreds of μm.

One way to produce droplets of consistently small size is to use an ultrasonic atomization process [37-39]. Atomization of the coating solution/suspension with the aid of a vibrating piezoelectric crystal provides the spray droplets of desired size and can accommodate the use of wide range of materials. Several companies, such as Sono-Tek, Sonaer, and Optomec are successfully using ultrasonic atomization processes to generate aerosols used for coatings and micro printing (in the case of Optomec). However, Sono-Tek and Sonaer spray nozzles can only be used for low frequency vibration (up to 130

kHz), which limits the diameter of the sprayed particles to a minimum of ~12 μm (in the case of water as a solvent). Furthermore, the above mentioned nozzles may require additional mechanism of spray acceleration to optimize the particle velocity at the impact. Optomec's micro printing equipment atomizes the solution in a separate chamber (hence higher frequency of vibration and smaller particle size) and uses so called "shroud air" to accelerate the particles pushed through a small diameter (order of ~100 μm) channel, which might cause clogging problems. Additionally, the Optomec system is designed primarily for microprinting and not intended to be used for large area coating.

The objective of this paper was to develop an innovative system for the spray coating and micro printing which will include an ultrasonic particle generation device and a nozzle for the spray deposition. The deposition nozzle, due to the larger diameter of the outlet channel, allows for a high throughput of droplets and simultaneously will accelerate and focus spray droplets using central high-speed air flow in the center of the nozzle exit. Therefore, the proposed system attempts to solve both, droplet size and uniformity and proper droplet impact velocity problems to achieve close to optimum coating conditions. The described design could be successfully used for large area coating, such as windows and solar panels, as well as micro printing of electronic circuits and numerous other applications.

2.2 Note on particle impact dynamics

To provide an optimum regime for the liquid particle delivery and application, we need to consider its size and velocity. The main parameters that determine the size of atomized particles are the frequency of the ultrasonic nebulizer, liquid density, and liquid

surface tension. The empirical formula that gives a fair estimate of the mean particle diameter is[40],

$$D_m = 0.34 * \sqrt[3]{\frac{8\pi * T}{\rho * f_a^2}}$$

where D_m is droplet diameter, T is liquid surface tension, ρ is liquid density, and fa is nebulizer frequency. Knowing the mean droplet size for a given nebulizer frequency, we can determine the corresponding desired velocity of the droplet, which will govern the droplet-surface interaction.

In general, there are three possible regimes of liquid droplet-solid surface interaction: spreading, rebounding, and splashing (see Figure 2-1). For a coating system consisting of a spray generation unit and an application nozzle, it is important to establish a rebounding regime within the system before the droplets exit the nozzle [40]. That will minimize the condensation of liquid on tubing/nozzle walls and unnecessary buildup of material on the internal surfaces.

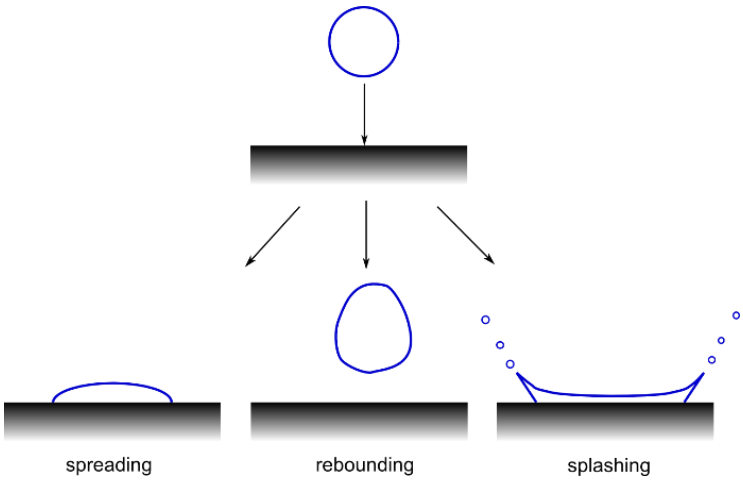

Figure 2-1. Modes of the droplet-surface interaction.

To ensure a non-stick condition or to control the particle impingement, a set of non-dimensional numbers is used. For the particle to rebound from the surface upon the impact, Weber number (*We*) provides the transition condition[41]:

$$We = \frac{w_0^2 D_m \rho}{T}$$

where D_m is mean particle diameter, T is liquid surface tension, ρ is liquid density, and w_0 is velocity normal to the surface. In order to provide rebounding regime for the travelling droplets to the nozzle, we must ensure that the condition $We<10$ is satisfied.

On the other hand, droplets on the target surface should neither rebound nor enter the splash regime (when the droplet will disintegrate into a number of smaller particles upon impact). To provide optimum distribution and adhesion of deposited material, droplets should spread on the surface forming a thin film. Therefore, another characteristic dimensionless number (K_m) is used to provide a guideline in the system design process. To prevent splashing, the condition $K_m<K_{mc}$ should be satisfied (where $K_{mc} = 57.7$)[32]. The formula used to compute K_m is

$$K_m = \left(O_h{}^{-2/5} * We\right)^{5/8}$$

where

$$O_h = \frac{\mu}{\sqrt{T * \rho * D_m}}$$

where O_h is Ohnesorge number and μ is liquid dynamic viscosity.

Therefore, to satisfy the rebound condition on the nozzle's internal surfaces as well as prevent splashing on the target surface, a dual-regime nozzle should be used. While a low velocity rebound regime is desirable on the internal surfaces of the device, droplets have to have higher velocities at the substrate surface to ensure a splashing regime to achieve

efficient deposition with minimal material waste. Moreover, by decoupling the particle generation device and the application nozzle, compared to pressure-based devices, much better control of the spray velocity can be achieved, which will be explained more in detail in the next section.

2.3 Design

2.3.1 Design concept and system development

The core of the design consists of the atomized droplet generation and the deposition nozzle decoupled in their respective operation. The low velocity carrier gas takes the droplets from the droplet generation unit to the deposition nozzle. At the nozzle exit, the particles are accelerated and focused by the high speed gas flow from the tube in the center of the nozzle. Therefore, a dual velocity regime is realized by using the lower velocity carrier gas internally, while the droplets are accelerated at the nozzle exit just before the deposition occurs. To avoid condensation, facilitate droplet size uniformity, and ensure symmetry of the particle stream, an extra intermediate flow-conditioning unit (FCU) was added to the design. FCU also doubles as a mixing chamber when two or more materials are deposited simultaneously (Figure 2-2).

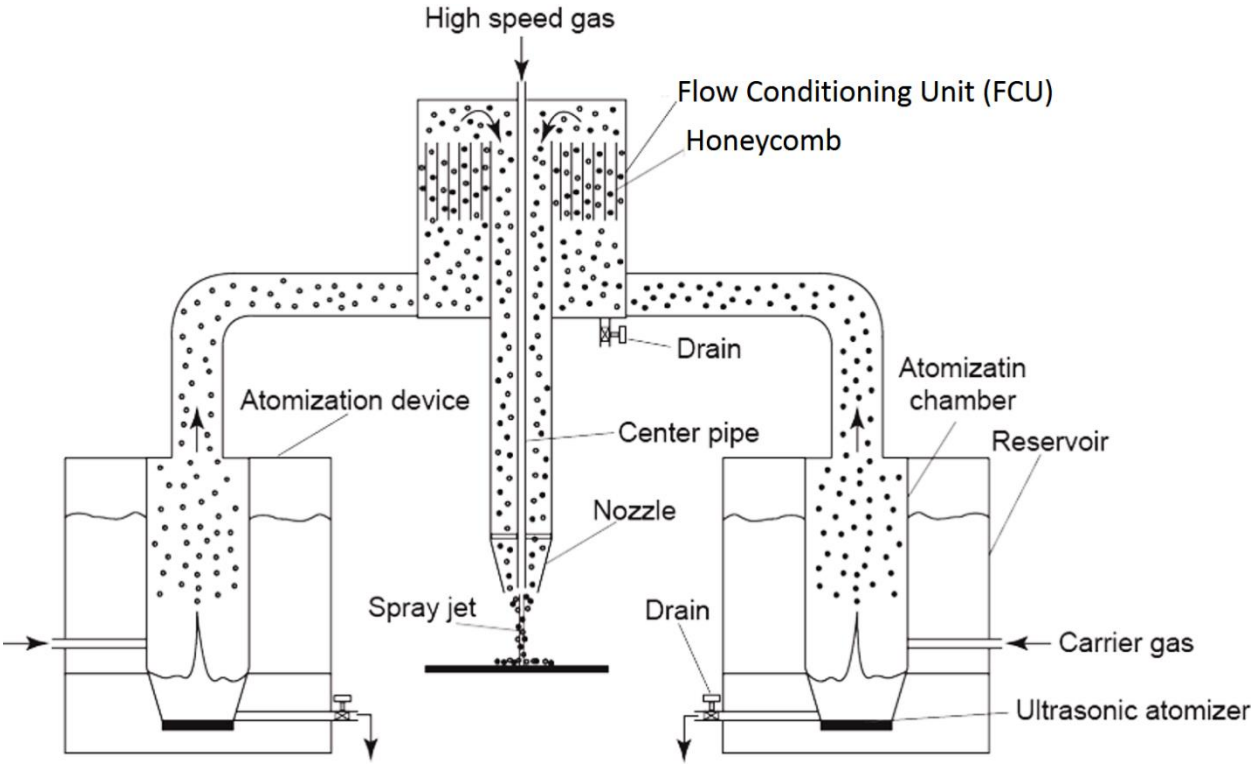

Figure 2-2. Nozzle with double atomizer schematics.

The FCU is placed in between the atomizer(s) and the nozzle and consists of a hollow cylinder with honeycomb structure imbedded in it. The asymmetric entrance ensures a vortex forming in the lower section to sort the particles. Due to a 'cyclone' effect, larger particles will collide with the wall of the chamber, condense, and will be drained out of the FCU. Smaller and lighter droplets will travel through the honeycomb and further down to the nozzle exit. The carrier gas stream is also made less turbulent while passing through the honeycomb structure. Furthermore, the FCU allows the addition of the long high-speed central gas tube, which creates an axisymmetric exit channel thus reducing turbulent disturbances within the nozzle and at the nozzle exit. A 3D model of the nozzle design and the fabricated nozzle mounted onto a CNC router (Romax CNC, USA) are shown in Figure 2-3.

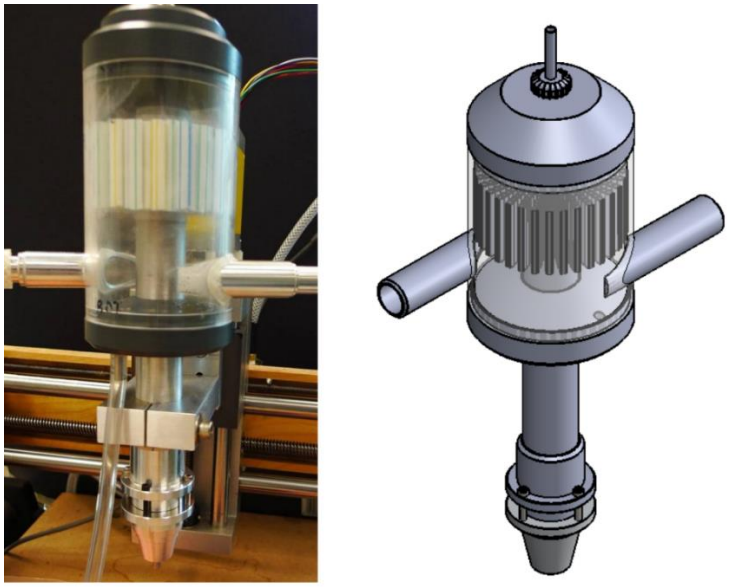

Figure 2-3. 3D model of the nozzle (right) and a nozzle mounted on a CNC router (left).

The nebulizer used was based on the APC International atomizer board with 1.65MHz piezoelectric element, rated input voltage of 48V, and mist output ratio of ~350cc/hr. The mist flow rate was set at 0.1-0.15 m^3/min to satisfy low velocity condition within the nozzle. The average droplet size was measured to be 6.0 μm with 1.65 MHz[42].

The exit jets of atomized droplets from the nozzle at different conditions are shown in Figure 2-4. The form of the exit jet is dependent, among other things, on the position of the high-speed center tube with respect to the nozzle exit. The "dome" at the nozzle exit is actually a stable vortical structure, as can be seen from high-speed imaging and described in more details in a later section. Figure 2-4 clearly shows that most of the atomized droplets are tightly focused into a high-speed jet. Consequently, the accelerated particles are deposited onto the substrate in such a way as to maintain close to optimum coating conditions.

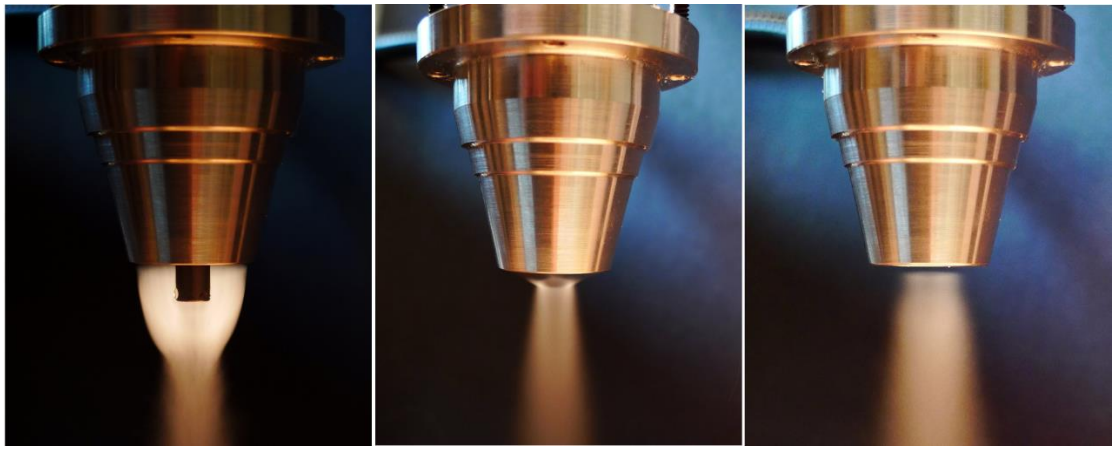

Figure 2-4. Exit jet: center tube out (left), center tube flash with nozzle exit (middle), center tube inside (right).

In order to produce a coating with droplets uniformly distributed over the substrate's surface, a series of experiments were conducted to determine close to optimal distance of the nozzle tip from the substrate. For a nozzle with an exit diameter of 15 mm, the distance was determined to be approximately 30-35 mm. As the nozzle was mounted on a CNC router platform, the feed rate (i.e. the lateral velocity of the nozzle motion across the surface) was also optimized. The combination of appropriate nozzle exit distance and feed rate produced a coating layer where the solvent was evaporated within 1-2 seconds after deposition. This rapid evaporation ensured that smaller droplets would not coalesce, thus providing the opportunity for the nanoparticles to settle on the surface before they could agglomerate into large clusters.

2.3.2 High speed imaging and PIV analysis of the resultant jet

To study the overall structure of the jet forming at the nozzle exit, a series of images using high speed recording equipment and PIV technique were analyzed. The near-field structure of a coaxial jet is considerably complex. The mixing between the jet streams is critically controlled by the dynamics and interactions of the vortical structures in shear-

layers developed between the two jets, and also between the outer jet and the ambient fluid. To study the effects of controlled perturbation, the inner jet was turned off and on, as illustrated in Figure 2-5 (a) and (b), respectively. In both cases, the jet propagated freely into the unbounded area until it impinged on a 3 mm plate, located 40.5 mm downstream. The images shown in Figure 2-5 were collected using particle image velocimetry (PIV). The PIV system, implemented to acquire quantitative images of the air flow across the cavity opening, consisted of an Nd:YLF dual cavity laser (power output of 22.5 mJ/pulse at 1 kHz, wavelength of 527 nm), which provided illumination of the flow field. The flow was seeded with Di-Ethyl-Hexyl-Sebacat (DEHS) droplets with a mean diameter of 1 μm. The particles were generated using a flow seeder that employed Laskin nozzles (model # 1108926, LaVision GmbH, Germany), which inject high velocity streams of compressed air into an oil bath. The air jets atomize the oil and produce a polydisperse oil aerosol. The particle concentration was controlled by employing a secondary air inlet to the atomizer, which contained a flow rate regulator. The Stokes number of the droplets ($St = \rho_p d_p^2 U/18\mu L$, where ρ_p and d_p are density and the diameter of the tracer droplets respectively, μ is the dynamic viscosity of the fluid, U is the droplet velocity, and L is a characteristic length) was equal to 2.8×10^{-3}, which indicated that the droplets were sufficiently small to accurately follow the flow. The images of the tracer droplets were recorded with a digital Complementary Metal Oxide Semiconductor (CMOS) camera equipped with a sensor that consisted of 1024 × 1024 pixels.

Initially, the center gas was turned off and the flow was allowed only through the outer region of the nozzle. As a result, the impinging jet formed for which the structure

can be visually separated into three main regions: R1 - Free jet region, R2 - Stagnation region, and R3 - Wall-jet region. When the center gas is not present, the large vortical structure, represented by a primary vortex, was periodically formed and shedded from the nozzle, as it can be seen in Figure 2-5(a). Spectral analysis of the temporal modes of the jet, obtained through proper orthogonal decomposition (POD), showed that the shedding frequency of these large vortical structures was about 137 Hz. As the flow is deflected from the impinging wall, a wall jet was developed. The wall jet separated due to the interaction with the primary vortices and the impinging wall, and as a result, secondary vortices, with shedding frequency of 235 Hz were formed. The interaction of the primary vortices with the wall shear layer gave rise to unsteady vortical motions. Additionally, the presence of the large vortical structures created a rather large impinging area of the jet, with the diameter larger than that of the nozzle.

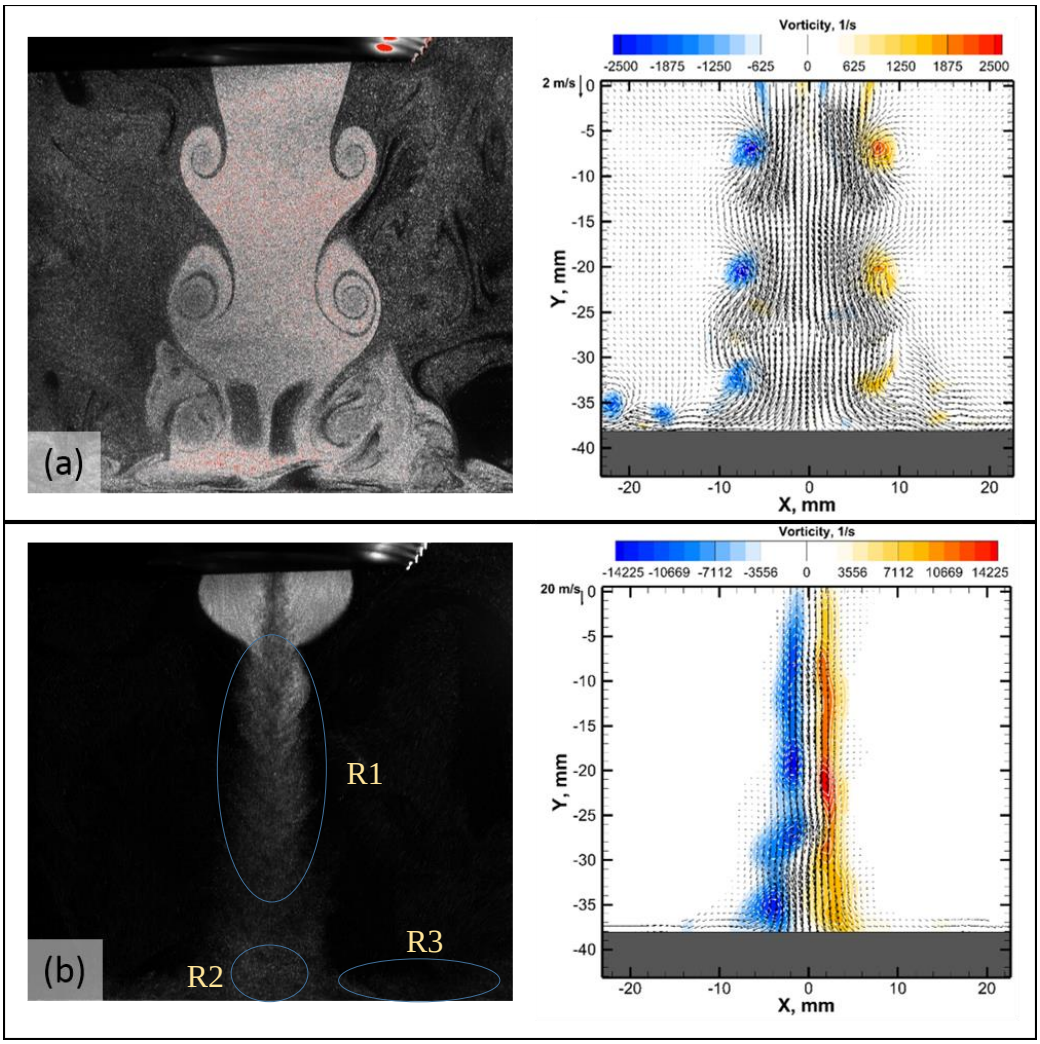

Figure 2-5. Flow patterns of the (a) jet with the mean circular jet velocity of U =3 m/s ; (b) coaxial jet with the mean center circular jet velocity, Ui = 35 m/s.

The introduction of the center jet led to the formation of a proper coaxial jet and changed the dynamics of the flow significantly. Because the vortices in the outer shear layer roll up, the vortices in the inner shear layers cannot be easily identified as separate entities. It can be seen from Figure 2-5(b) that vorticities are connected to each other, indicating that three-dimensional effects are of prime importance for the vertical structure. Spectral analysis of the temporal modes of the coaxial jet showed that the vortical

structures with shedding frequency of 215 Hz and 274 Hz dominated the flow field, with the lower frequency corresponds to the outer jet and the higher frequency corresponds to the center or inner jet, respectively. The presence of the inner jet led to a substantial decrease of the all three regions of the impinging jet and allowed it to focus the coaxial jet on a much smaller area, compared to that in the previous case.

2.3.3 Uniform coating performance testing

In order to test the uniform coating distribution performance of the nozzle, a number of coating experiments were conducted. These experiments indicated that the nozzle design allows for the particles to be uniformly deposited onto a variety of substrates with different geometries.

2.3.3.1 Encapsulated silica

Polymer-coated silica nanoparticles were coated onto glass a substrate with subsequent sintering at 500^{o}C for 4 hours. Nanoparticles used in this experiment were Vive Nano Silica (+) (by Vive Nano, Canada) polymer encapsulated silica nanoparticles (water based suspension with 0.1% of nanoparticles by weight). Results shown in Figure 2-6 indicate a uniform thickness with a very slight variation in the range of about 10 nm. The image was taken using Hitachi S-4800 field emission scanning electron microscope and QUARTZ PCI (version 8) software. The polymer used to encapsulate the particles is evaporated during the sintering process. The remaining nanoparticles form a coherent layer sufficiently covering the substrate with no observable gaps in the coating.

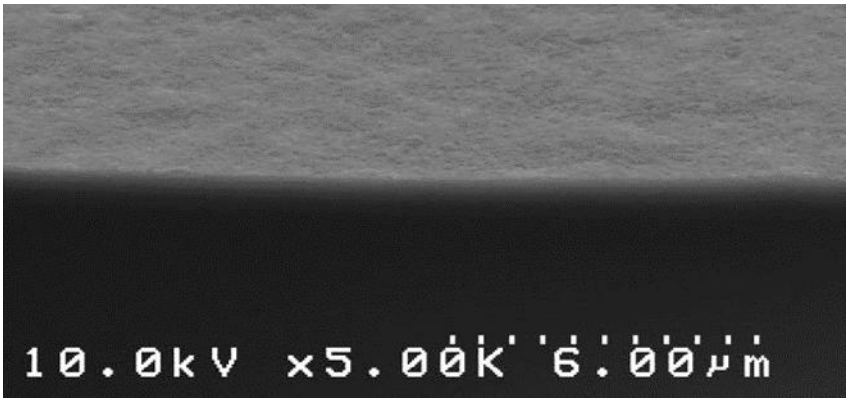

Figure 2-6. The edge of silica coated glass slide.

2.3.3.2 EDX results pure silver on glass

Pure silver nanoparticles were also deposited onto a glass substrate. To highlight the distribution of the nanoparticles on the substrate, an EDX analysis has been performed (Hitachi S-4800 SEM). The resultant spectrum and the accompanying mapping image are shown in Figure **2-7**. EDX results clearly show that silver nanoparticles are evenly dispersed on the glass substrate surface. The particles were synthesized in house and the average is around 20-30 nm in size. The modified polyol process was used to synthesize the nanoparticles [43].

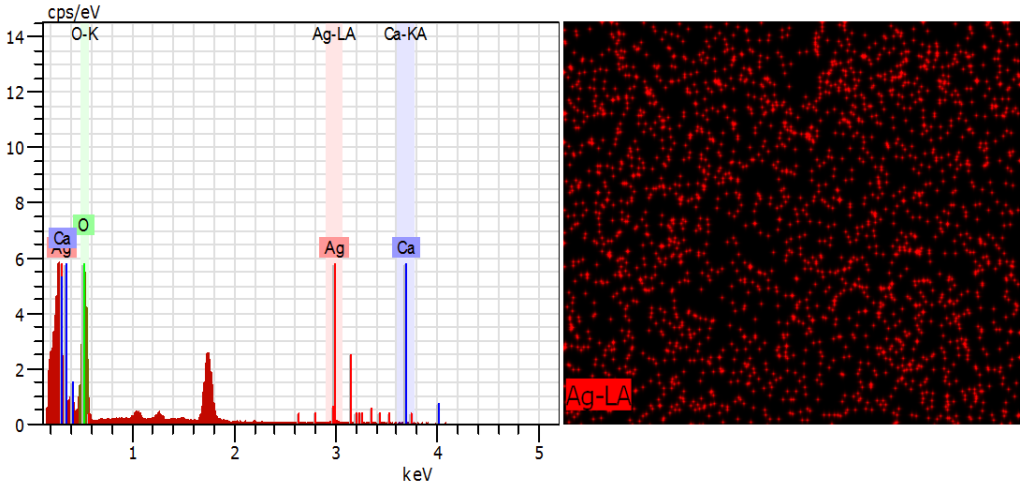

Figure 2-7. EDX analysis results: spectral analysis (left), and mapping of silver particles (right).

2.3.4 Dual inlet test

To verify that the dual inlet design produced a uniformly dispersed mixture of the two different nanoparticle suspensions, coatings with two acrylic inks of green and red color containing around 100 nm sized pigments were applied onto a glass substrate. The resultant coatings were examined using an optical microscope (Zeta-20 optical profiler, Zeta Instruments, USA). The red pigmented ink was first used to coat a glass substrate; then, the green pigmented ink was used to coat a different glass substrate. In order to test the on-the-fly mixing capability of the FCU unit in mixing of two sets of droplets generated by two independent atomizers, the red and green pigmented inks were atomized simultaneously by two different atomizers and the two sets of droplets were mixed at the FCU unit. Then, the mixture of droplets were sent to the nozzle for coating. The acrylic pigmented inks used were Daler Rowney FW acrylic ink in red and green and were diluted to 5% with distilled water. Comparison of the samples coated with red ink, green ink, and dual coated glass is seen in Figure 2-8. Although there are no brown color pigments used (only red and green), because of the presence of red and green pigments uniformly distributed on the substrate, the coated mixed pigments show brown color. This confirms the uniform on-the-fly mixing capability of the FCU unit and indicates simultaneous deposition possibility of foreign nanoparticles that might not mix well in solution.

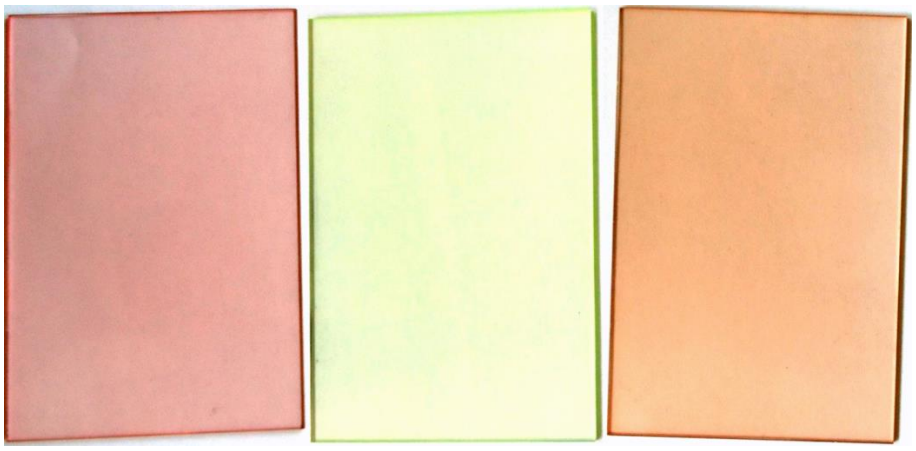

Figure 2-8. Coated glass: red ink only (left), green ink only (middle), mixed pigments (right).

A closer look at the coating uniformity using optical microscope reveals that the pigment nanoparticles are evenly dispersed over the coated surface (see Figure 2-9). These results also confirm the assumption that the small droplets containing ink pigment particles will evaporate during the coating process before they would have the opportunity to form larger droplets on the coated surface.

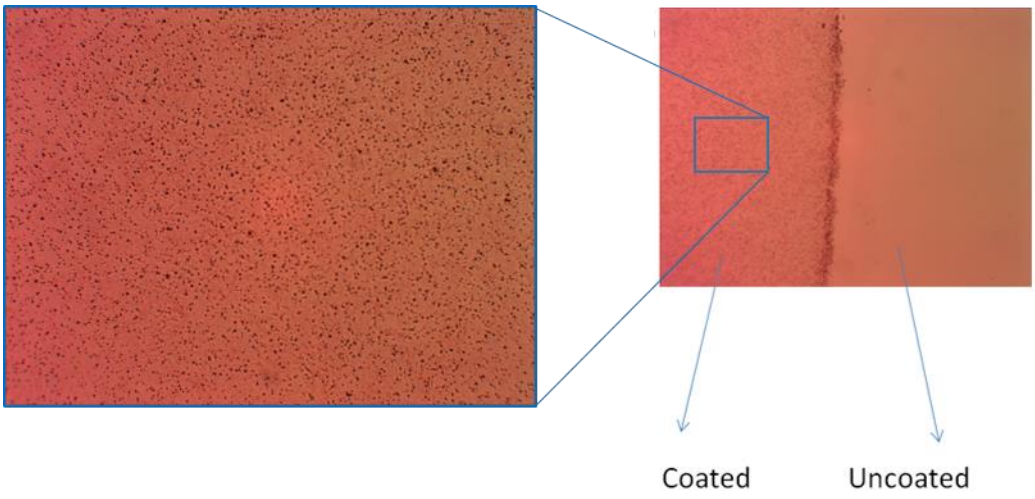

Figure 2-9. Dispersion of ink pigment particles on glass.

2.4 Applications and Results

Due to the system's inherent adaptability, the number of possible applications is quite large as various coatings are used extensively throughout industry and in many research areas. Some of the possible applications the system was adapted to be used in are illustrated in subsequent sections.

2.4.1 Printing

First attempts in using the initial design of the system were done in micro-printing. Because the atomization function was removed from the nozzle design, it is relatively much easier to downscale the design for micro-printing. Figure 2-10 shows printed lines of ~80 μm in width, printed using a miniaturized nozzle. Although the system was not specifically designed for micro-printing but was only downscaled, the results clearly showed its potential to be used in micro-printing.

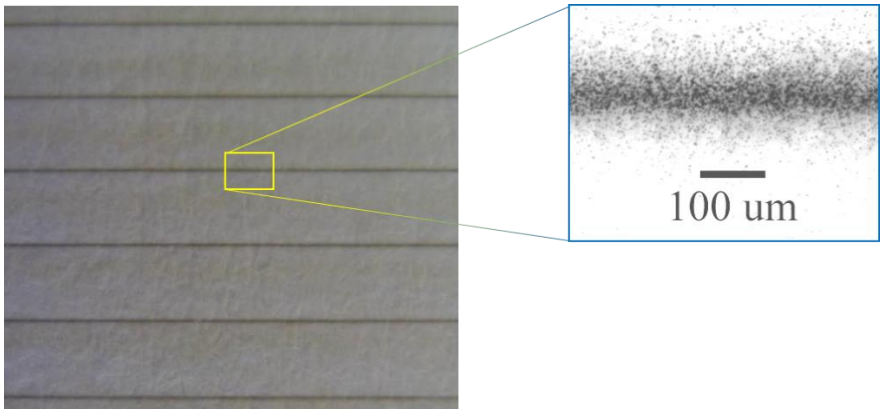

Figure 2-10. An example of printed line.

2.4.2 Antireflective coating

The coating system was also used for antireflective (AR) coating applications. Antireflective (AR) coating applied with the coating system showed significant

improvements as far as the light transmission and reflection spectrum is concerned. AR coating consisted of subsequent layers of TiO_2 and SiO_2 films of approximately 100 nm thickness each. Figure 2-11 illustrates a schematic of how these films are applied to achieve an AR function as well as the refractive index values of each material. The coated surface was subsequently sintered at 550 ^{0}C for 4 hours to remove the polymers encapsulating the nanoparticles. Subsequently, the transmittance spectrum of the coated samples was measured using an Ocean Optics USB4000 spectrophotometer equipped with a DT-MINI2 light source. The AR coating results are shown in Figure 2-12. Evidently, words behind the glass slide can be seen much better through the coated area, whereas, due to light reflection, it is not as easy to see the words through the uncoated area. Figure 2-12 (right) also shows the uniformity of the coating thickness including both TiO_2 and SiO_2 coatings; only a few nm variations can be observed in the SEM image of the coating. The surface roughness values (Ra) of the resultant coating were measured to be between 0.035 and 0.04, compared to the gold sputtered surface roughness of ~0.02.

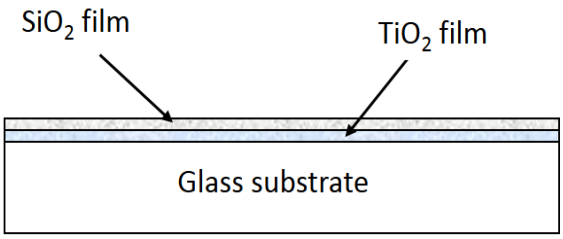

Material	Refractive index (n)
Air	1.0
Glass	1.5
TiO2	~2.5
SiO2	1.47

Figure 2-11. Coating schematic and refractive indexes of coating materials, substrate and air.

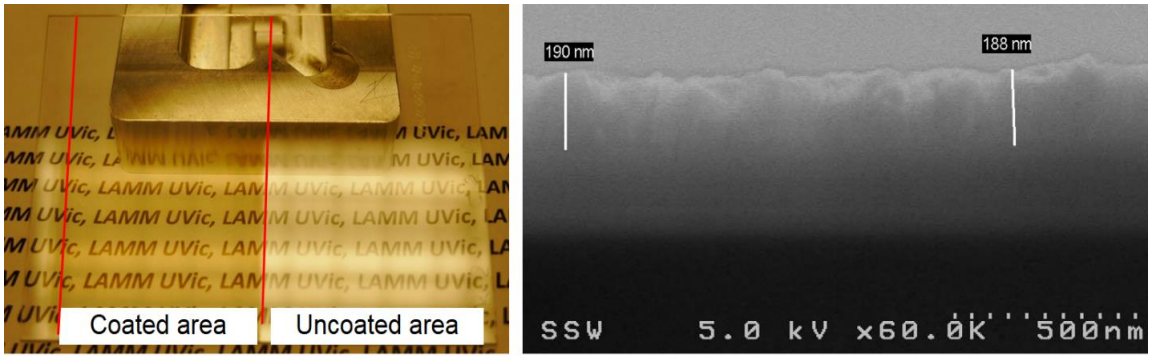

Figure 2-12. Comparison of the coated vs uncoated glass sample (left); SEM image of the coating`s cross section.

Furthermore, the coating system proved to be highly adaptable to varying surface geometry such as the interior surface of a glass tube. Figure 2-13(right) depicts the coating system used in AR coating of the inner surface of a glass tube of 1.5" diameter. A horizontal coating nozzle was designed and fabricated for this purpose as shown in Figure 2-13 (left) in order to be able to coat the tube interior surface. The coating process involved simultaneous motion of the nozzle along Z-axis at 4.0 in/min and tube rotation at close to 60 RPM. The tip of the nozzle is situated approximately 5 mm from the inner tube surface. Similar to flat glass samples, the tube was heated to 550^0C for 4 hours to remove the polymer encapsulating the nanoparticles. The resulting transmittance spectrum through the wall of the tube is shown in Figure 2-14. As shown, light transmission is improved over the coated tube due to the AR coating.

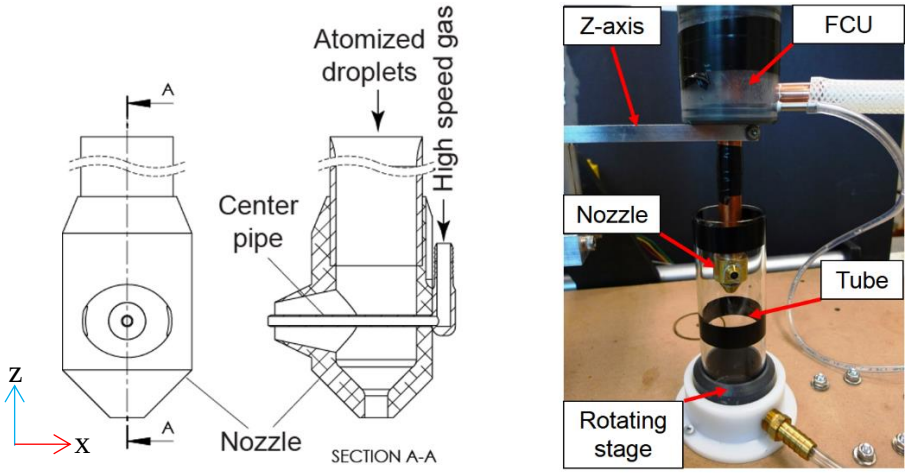

Figure 2-13. Curved surface coating: nozzle cross section (left), coating setup (right).

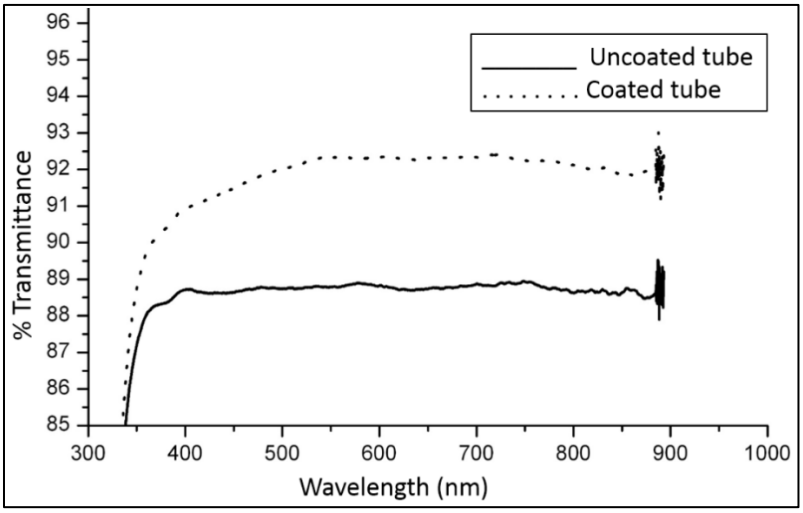

Figure 2-14. Transmittance spectrum comparison of coated and uncoated tube.

2.4.3 Coating for Improved 3D Scanning

Optical 3D scanning techniques are widely used in industry, research, archeology, and other fields for creation of digital solid models of physical objects. Some optical 3D scanning techniques, however, can struggle to obtain accurate representation of surfaces because optical scanning is difficult over shiny or black surfaces. In most cases, the object to be scanned is coated with materials of better optical property using a spray can

or spray gun. However, conventional spray coating techniques often cause over-spraying, excessive layer thickness, and “blind” spots in difficult to reach areas.

Because coating for optical 3D scanning is typically done manually, a hand-held nozzle was designed for use with atomization coating system as can be seen in Figure 2-15. This nozzle was used to improve the ability of the scanner to create an accurate 3D surface by applying a thin coat of opaque paint. The hand held nozzle has a trigger valve that activates a high speed gas jet to focus and accelerate the spray supplied from the atomizer. Therefore, it can be used in much the same way as a conventional spray gun.

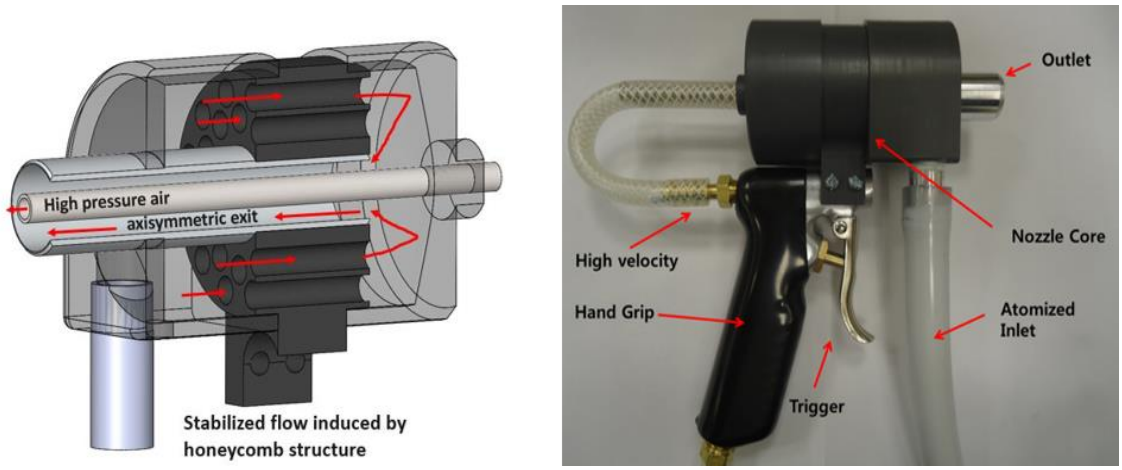

Figure 2-15. Handheld nozzle for improved 3D scanning: 3D model (left), and assembled nozzle (right).

A comparison of the effectiveness of the proposed system with the conventional spray, showed that the developed nozzle configuration is capable of producing scanning results that more accurately represent the actual physical object. A machined aluminum part was coated with the proposed system as well as using a conventional method utilized in 3D scanning as shown in Figure 2-16. After being sprayed, the part was scanned using a HDI Blitz structured-light 3D Scanner with accuracy of approximately 120 µm. As is

commonly done, several scanning passes resulted in an image of the coated surface comprised of a point cloud. The scanning results are shown in Figure 2-17. As can be observed, the corner that was coated with the proposed system matched the actual geometry of the part much better than the conventionally coated one. Also, some air pockets can be seen over the conventionally coated corner area. This result can be explained by a significantly thinner layer of coating on the surface, hence a minimal change to the part geometry resulting in a more accurate representation of the actual part. The coating thickness on the flat portion of the part was recorded as ~10 µm for conventional coating versus ~0.2-0.4 µm for the proposed coating system. The surface roughness (Ra) recorded for the conventionally coated sample was approximately 0.3, whereas the coating applied with the system gave a much lower value of ~0.04.

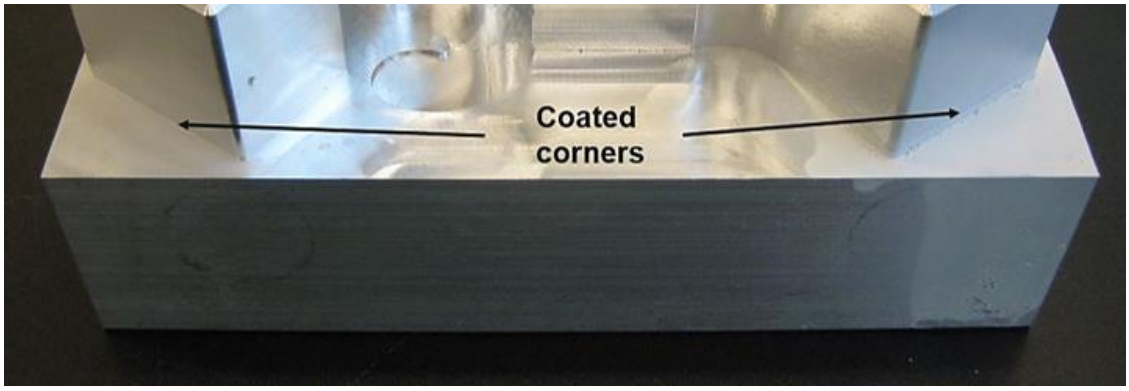

Figure 2-16. A coated part: Spray coating system (left); Conventional spray canister coated (right).

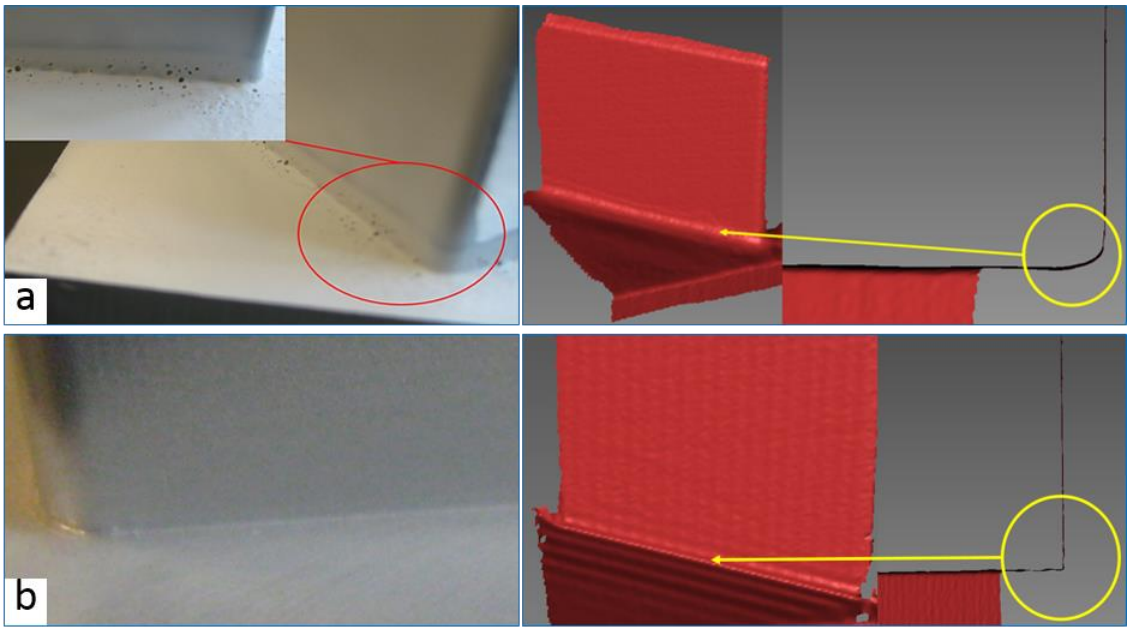

Figure 2-17. Sprayed and scanned aluminum part coated with conventional (a) and proposed coating method (b).

2.5 Conclusion

In this manuscript a coating system is presented and its performance is tested and analysed for different coating applications. The core principle of the system's operation is the decoupling of the droplet generation device and the nozzle that facilitates close to optimum coating conditions. A dual regime nozzle ensures the particles travel through the nozzle at relatively low velocity to prevent particle adhesion to the interior walls. At the same time, at the exit of the nozzle the particles are accelerated to enter the "spreading" regime as outlined in the particle impact dynamics section. The unique tunability and adaptability of the system configuration allows nozzle design changes suitable for a number of different coating applications. The potential of the system to be used in conventional spray coating and micro printing have been demonstrated.

Chapter 3 **Uniform silver nanoparticles coating using dual regime spray deposition system for superhydrophilic and antifogging applications**

This paper was published in Journal of Coatings Technology and Research in 2017. Maxym Rukosuyev, Ahmad Esmaeilirad, Syed Baqar, and Martin Jun." Uniform silver nanoparticles coating using dual regime spray deposition system for superhydrophilic and antifogging applications", Journal of Coatings Technology and Research, 14(2), (2017), pp. 347-354.

This chapter describes the process of using dual velocity deposition nozzle to produce uniform sub-micron thick layer of silver nanoparticles to create antifogging and antireflective effect on glass surface. The scope of this chapter include updated nozzle design and its potential application in coatings on optical devices.

Contributors:

Maxym Rukosuyev – designed, manufactured, tested the coating system, and completed the manuscript.

Ahmad Esmaeilirad – synthesized materials (silver nanoparticles) used in coating experiments and helped in compiling the corresponding section of the manuscript.

Syed Baqar – helped in conducting the experiments, data recording, and analysis.

ABSTRACT

Antifogging and/or superhydrophilic properties of coatings are widely exploited both in a lab environment and in industrial applications. Material choice for the production of the said coatings is of vital importance for the final coating properties. Silver nanoparticles have been known to have antibacterial and fungicidal properties, which make them extremely useful in biomedical applications. Production of coatings that combine superhydrophilic and the unique properties of silver nanoparticles can be beneficial in numerous applications. Dual regime spray coating system allows the

production of thin, uniformly distributed nanoparticle coating through droplet impact velocity and gas flow control. Silver nanoparticles of ~15nm average diameter were synthesized and coated onto the glass substrate, which produced the top layer with strong superhydrophilic/antifogging properties with water contact angles of close to 6 degrees. In addition, coated surfaces exhibited an increase in light transmission of ~0.7% in 500nm-700nm range.

3.1 Introduction

Superhydrophilic coatings are used extensively both in industry and active research. The applications for the surfaces exhibiting superhydrophilic properties include anti-fogging, drag reduction, enhanced heat transfer, anti-fouling, anti-reflection, biologically clean surfaces, and self-cleaning surfaces [6, 44, 45]. Some specific applications in biomedical field include the use of superhydrophilic surfaces to enhance antifogging properties of medical imaging devices [46, 47], increased resistance against absorption of proteins, bacteria, and fibroblast cells [48-50], reduce thrombosis [51], and improve bone healing and osteogenesis [52] among others. However, the production of superhydrophilic surfaces, in some cases, requires the use of a specific stimuli to trigger superhydrophilisity. Titanium dioxide and zinc oxide coated surfaces, for instance, can produce superhydrophilic effect when activated by UV light [44, 45, 53] and will lose their properties once being unlit for a prolonged period of time. Other stimuli include the use of mechanical stress, electric potential, and change in temperature to name a few [45, 54-57].

Silver nanoparticles have several attractive properties that make them useful in a number of applications. The use of silver nanoparticles for their antibacterial [58-60] and

antifungal [61-63] properties is widely accepted and described in literature. Incorporating silver nanoparticles into SiO_2 coatings [64] or using it directly on the Si substrate [65] produces antireflective effect which can significantly increase the efficiency of electro-voltaic solar cells. The unique combination of bactericidal, fungicidal, and superhydrophilic behaviour of the obtained coating may prove to be a considerable benefit in a number of biomedical applications. Furthermore, superhydrophilic properties of the obtained coating do not require activation of any sort, hence the coated parts can be stored securely and used immediately with no further treatment.

A number of techniques can be used for coating application. Conventional air pressure atomising nozzles often used for spray coating [34-36]. However, air atomising nozzles should have certain air pressure to ensure atomisation which limits the range of spray velocities that can be controlled. Moreover, droplet size distribution is strongly dependant on the pressure applied, and generally in the region of tens to hundreds of μm which limits the uniformity and thickness control when used over large area. Some companies, such as Sono-Tek, Sonaer, and Optomec are successfully using ultrasonic atomization processes to generate aerosols used for coatings or micro printing. These nozzles however, may require additional mechanism of spray acceleration to optimize the particle velocity at the impact and may suffer from internal condensation/clogging problems.

This manuscript describes a technique of silver nanoparticles deposition using a dual velocity nozzle in combination with the ultrasonic atomizer. That method allows fine droplet velocity and coating thickness control, eliminates clogging and condensation problems, and allows for uniform coating over a relatively large area. The atomizer produces a fine mist of droplets measuring approximately 3um-7um in diameter. Each

individual droplet contains a small number of nanoparticles from the suspension that has been atomized. When deposited onto the substrate (in this case glass), the liquid rapidly evaporates leaving a thin, uniformly dispersed layer of silver nanoparticles. Furthermore, to the best of our knowledge, silver nanoparticles have not been used to produce superhydrophilic/ antifogging coatings described in this manuscript. Antireflective properties of the obtained coating can also contribute to its usefulness in the applications where increased light transmission is desirable.

3.2 Materials

Spherical and mono-dispersed silver nanoparticles were synthesized by the polyol process [66, 67]. Materials used during the nanoparticles synthesis are silver nitrate (≥99%), ethylene glycol (anhydrous, 99.8%), and polyvinylpyrrolidone (PVP) (Mw ~29000) from Sigma-Aldrich. Initially, 4.5g of PVP was dissolved in 50 ml of ethylene glycol. The solution was stirred vigorously and heated up to 160°C in a silicone oil bath. Subsequently, silver nitrate aqueous solution (2.5g silver nitrate dissolved in 50 ml ethylene glycol) was drop-wisely added to the PVP solution. The mixture was maintained for 30 min at 160°C, with subsequent cooling to room temperature (~23°C). Silver nanoparticles were separated from the solution by centrifugation and washed in ethanol six times. Finally, silver nano-particles were dispersed in D.I. water to use in the coating process.

Transmission electron microscopy (TEM) imaging was taken using JEOL JEM-1400 transmission electron microscope. X-ray diffraction (XRD) measurements were performed on a Rigaku Miniflex diffractometer with a chromium source (kR radiation, λ = 2.2890 Å). Figure 1 shows the TEM images of silver nanoparticles with sizes ranging

from ~5 nm to 20 nm in diameter and illustrates size uniformity of monodispersed nanoparticles.

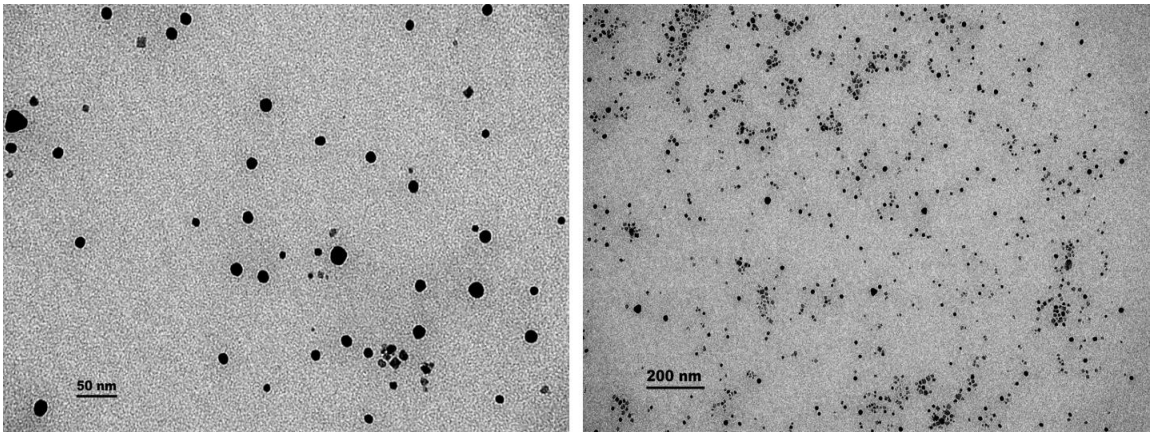

Figure 3-1. TEM images of synthesized Ag particles.

XRD analysis shown in Figure 3-2 confirms silver nanoparticles crystal structure (face centre cubic with Fm3m symmetry) with average crystallite size of 14.8 nm. The crystallite grain sizes of the silver nano-particles are calculated by the Debby-Scherer's equation [68]:

$$d = \frac{0.9\,\lambda}{\beta \cos\theta}$$

where d is the mean crystalline size, λ is the X-ray wavelength, β is the full width at half maximum (FWHM), and θ is the diffraction angle.

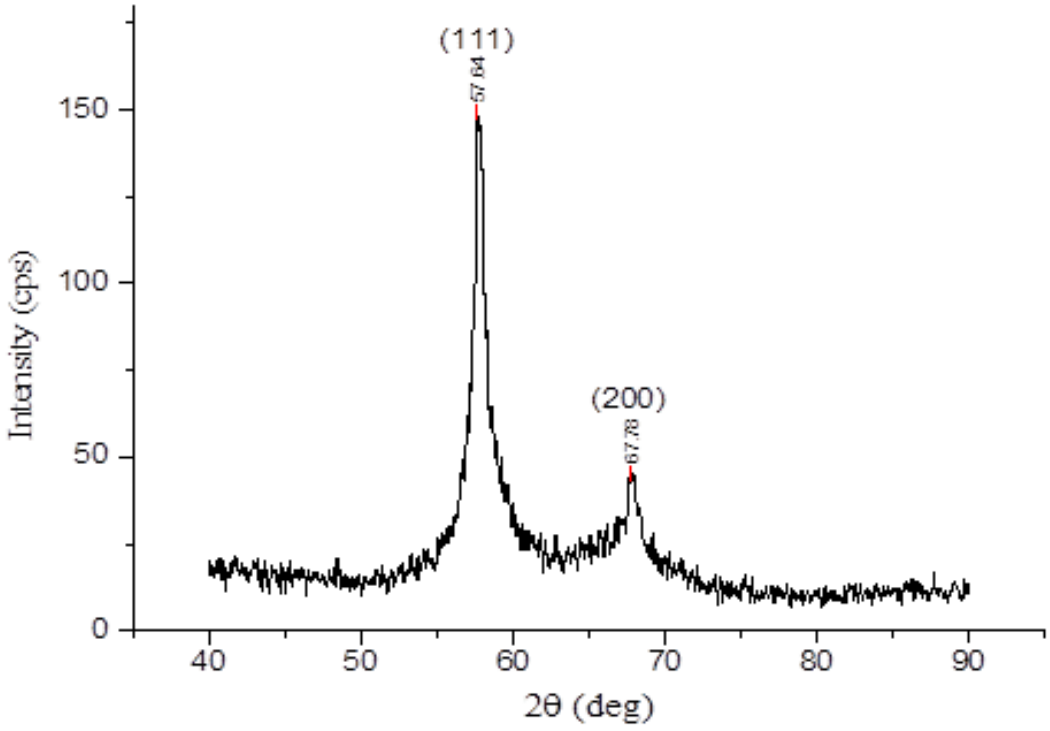

Figure 3-2. XRD analysis results.

3.3 Dual Regime Spray System for Coating

The device used to create the coating consists of an ultrasonic atomizer (2.4 MHz oscillation frequency), dual velocity deposition device developed in-house, and CNC router (Romaxx CNC Systems). The nozzle was mounted onto the router to ensure consistent coating application with set overlap, feed rate, and distance from the nozzle tip to the surface to be coated. A schematic image of the coating system is shown in Figure 3.

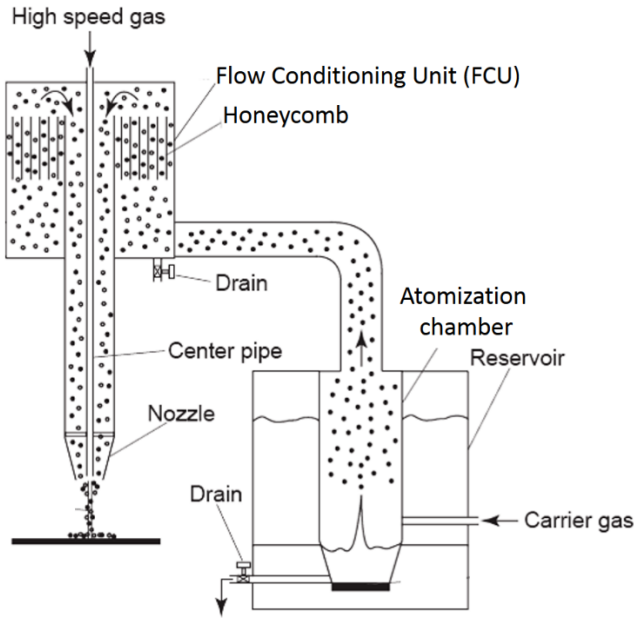

Figure 3-3. Deposition device schematics.

Silver nanoparticles suspended in water are atomized by the ultrasonic atomizer that produces a mist of water droplets with the average diameter of approximately 5 µm. Nanoparticles entrapped within the atomized droplets are carried to the deposition device by carrier gas stream (air in this case) at velocities of approximately 5 – 7 m/s. The 3D model of the deposition nozzle is shown in Figure 3-4.

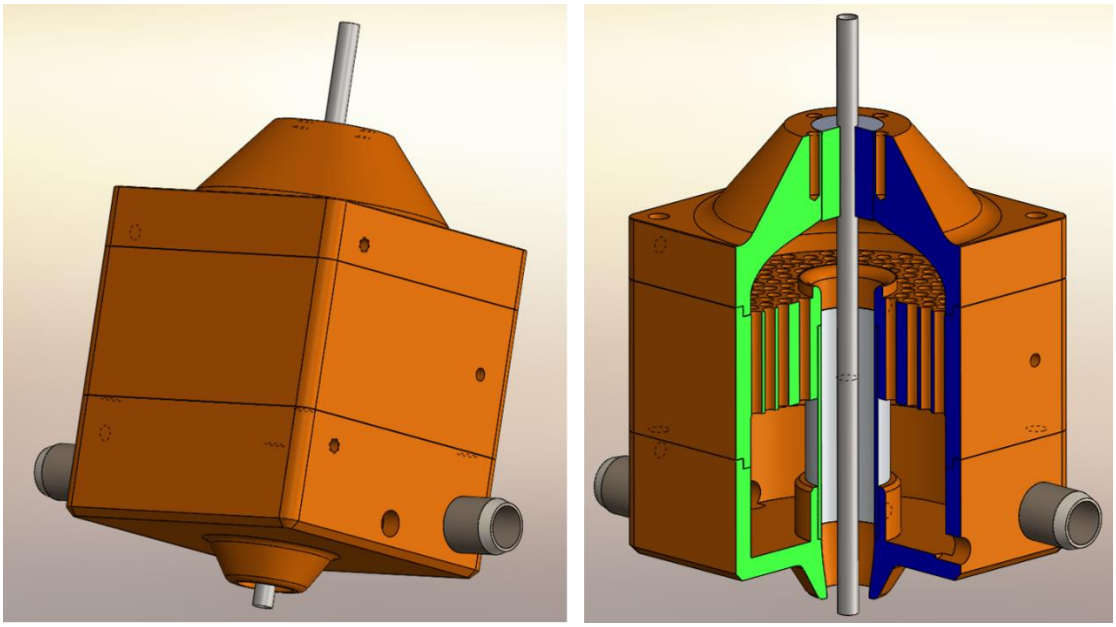

Figure 3-4. 3D model of the nozzle.

The dual velocity deposition setup ensures that the atomized droplets travel at relatively low velocities within the device as to ensure “rebounding regime” for the droplet/solid wall interaction [32, 41]. Simultaneously, droplets are focused and accelerated at the nozzle exit by using high speed air supplied through the center pipe to enter the “spreading” regime at the surface. Therefore, the device facilitates near ideal conditions for droplet deposition at the surface while significantly reducing the condensation on the internal parts of the apparatus. Further details on the coating system design and performance can be found elsewhere [27].

Spray coating was performed with 42 inches per minute of feed rate at a distance of 15 mm from surface. Liquid volumetric flow was measured to be ~.15ml/min, and the jet velocity at the surface was ~30m/s. The carrier gas flow, high-speed gas flow, and feed rate were adjusted in such a way as to allow for quick drying of the deposited material. That minimizes the formation of larger pools of liquid and agglomeration of nanoparticles on the surface. At the same time, the goal was to maximize the deposition

rate at optimum droplet impact velocities. Lower feed rates or shorter distance from the surface results in larger droplet formation which leads to visibly varying colouration of glass slide, non-uniform antifogging performance, and reduced transmission values. For higher flow rates, splashing of liquid on the glass slide is observed which again leads to the visibly varying colouration and reduction of deposition rates.

Coating was performed in an overlapping (50%) zigzag pattern with one section of the glass slide masked off for reference measurements. The distance between consecutive coating lines in the scan pattern was set to ~5mm. The distance is device specific and allows for uniform surface coating with no apparent areas of higher/lower coating densities.

3.4 Results

3.4.1 Coating characterization

To examine the morphology of the obtained surfaces, a series of images was taken with an optical microscope (Zeta-20 optical profiler, Zeta Instruments). Figure 3-5 shows an image of the coated surface at 100X magnification. As can be seen, nanoparticles are evenly distributed over the surface of the sample with some apparent agglomeration due to multiple coating layers deposited in order to facilitate imaging with optical microscope.

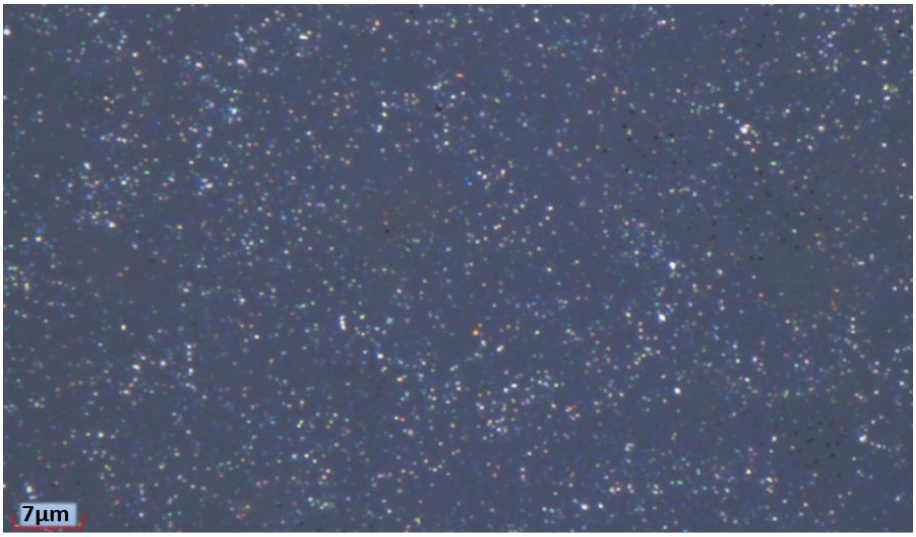

Figure 3-5. Optical microscope image of coated glass sample (100X magnification).

For higher resolution images, a scanning electron microscope (Hitachi S-4800 field emission scanning electron microscope) was used. The coated sample and the corresponding SEM image are shown in Figure 3-6. The coated samples shows light brown color due to the presence of silver coating on the surface. The SEM image of the surface shows that the coating appears to be uniform with only minor contamination on the surface from sample handling. In order to verify the uniformity of the coated silver nanoparticles, X-ray spectroscopy was performed on the same specimen using Bruker Quantex EDS system at 6 kV. The spectrum maps (220X) in Figure 3-7 confirms a uniform layer of silver nanoparticles.

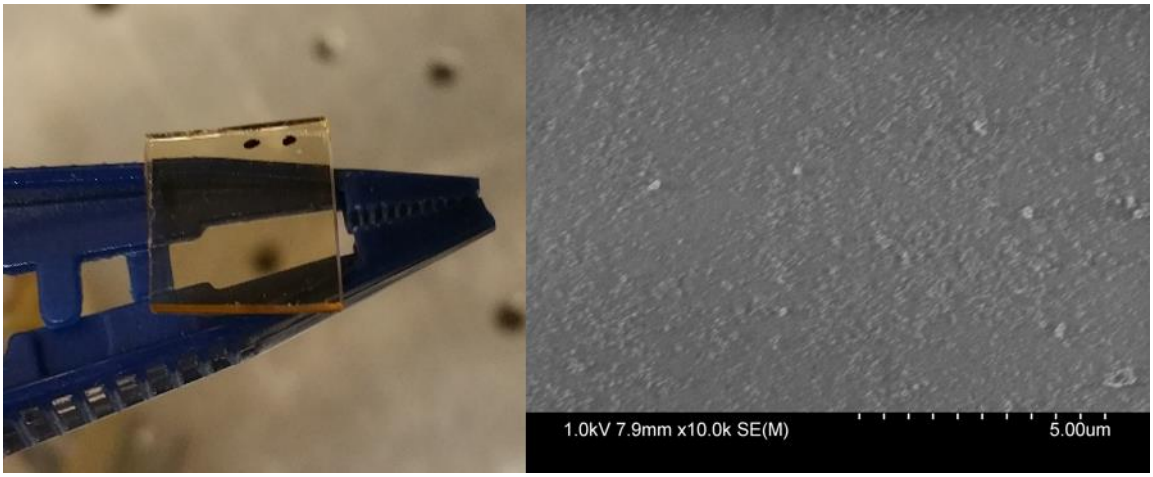

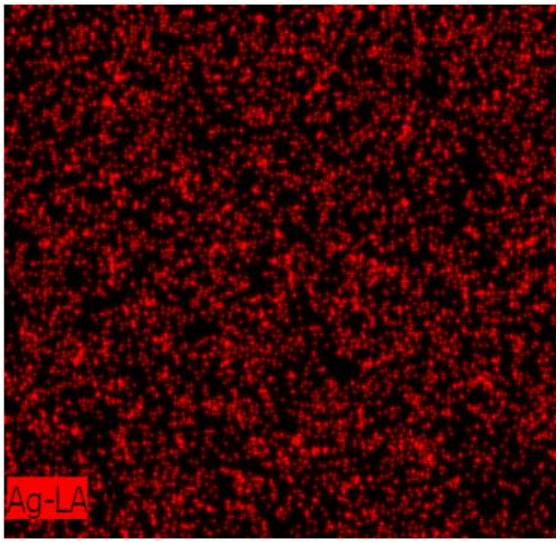

Figure 3-6. Coated glass sample (left), and SEM image of the resultant silver coating.

Figure 3-7. X-ray spectroscopy results from coated sample showing Ag map.

3.4.2 Superhydrophilic properties

Figure 3-8 shows the difference in water contact angle (measured with Holmarc HO-IAD-CAM-01B goniometer) between coated and uncoated glass sample. The contact angle of 2 microliter water droplet measured on the coated surface dropped from 17 degrees to ~6 degrees in about 4 seconds. The diminishing contact angles are plotted against time in Figure 3-9. These results clearly show the superhydrophilic nature of the

coating when compared with the water contact angles on the uncoated glass slide, which exhibit a decline in contact angle from 34 degrees to about 20 degrees and remain stable.

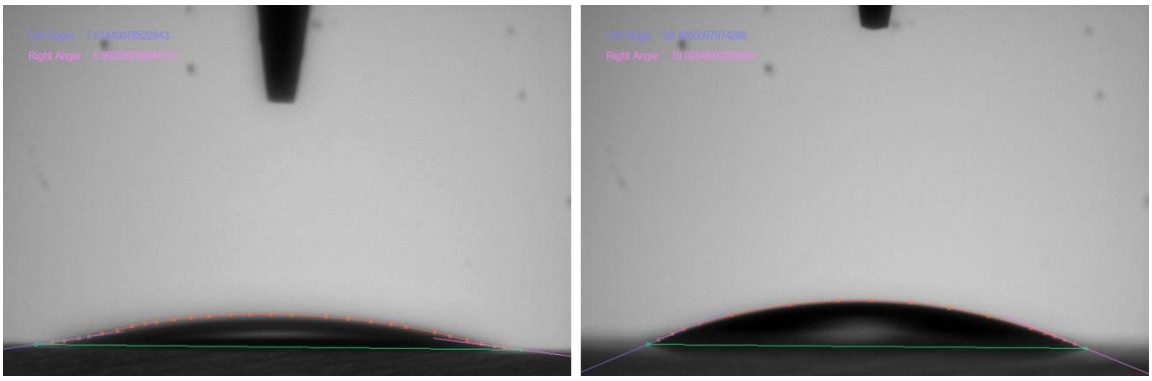

Figure 3-8. Water CA measurement on glass: coated (left), uncoated (right).

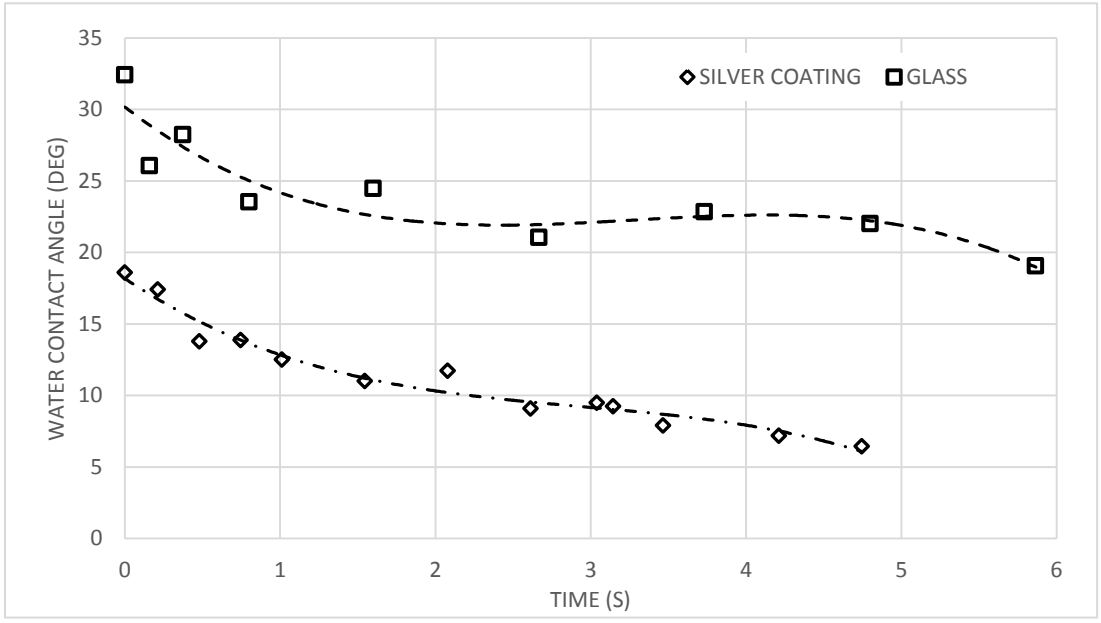

Figure 3-9. Water contact angle reduction on coated vs. uncoated glass surface.

Being superhydrophilic with fast CA decline times, the samples also exhibited antifogging properties. A half of a glass slide was coated with silver nanoparticles, and to verify the antifogging property, both uncoated and coated sides of the glass slide were exposed to steam by placing the slide above boiling water. As can be seen in Figure 3-10,

when exposed to water vapors in steam, due to condensation of these water vapors into droplets, the uncoated portion became foggy. However, on the coated portion, due to the superhydrophilic property, condensation resulted in thin water film, and the coated glass retained its optical transparency as shown in Figure 9. The coating was exposed to steam during 3 cycles of 5 minutes each while images were taken. The durability of coating's antifogging properties proved to be relatively stable (i.e. the antifogging effect was present after multiple cycles of steam exposure). The adhesion quality of the coating was not tested and will be the subject of further studies.

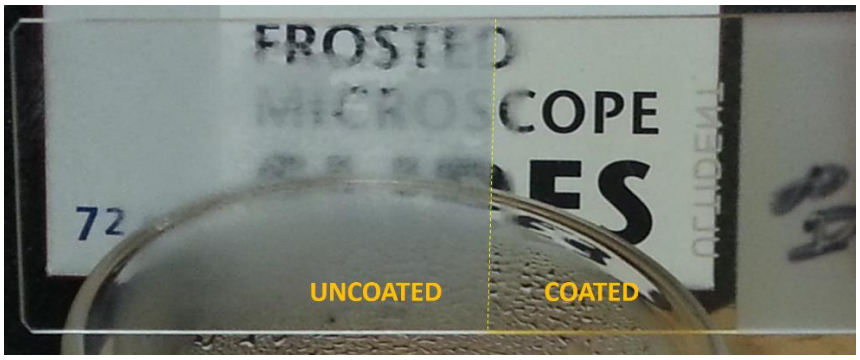

Figure 3-10. Antifogging effect on glass held above boiling water.

Light transmissions of the coated samples in dry condition as well as when exposed to steam were also measured to confirm antifogging property of the coating. The results were compared to those with uncoated samples as well. The light transmission was measured using a reflectometer (SR300RT, Angstrom Sun Technologies). Figure 3-11 shows light transmission measurement in the visible range through uncoated and coated glass slides under dry condition. As can be seen, slightly increased transmission is observed with the coated glass slide. This indicates that even under dry condition, the silver nanoparticle coating shows antireflective property. The average increase in

transmission of coated versus uncoated dry samples amounted to approximately 0.7% within 500 – 700 nm range.

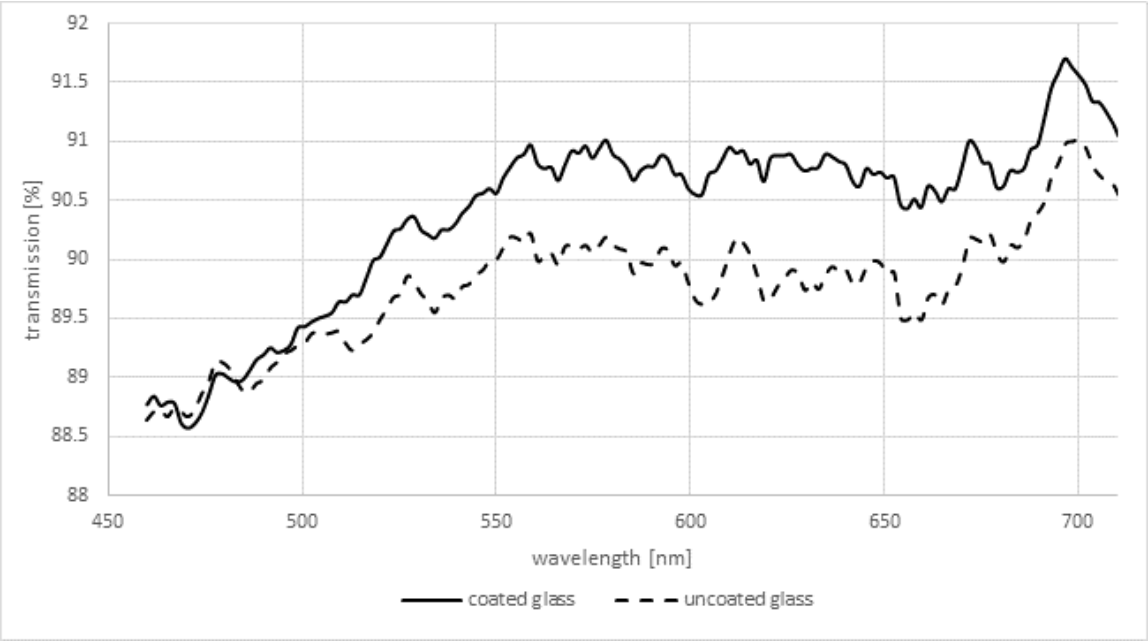

Figure 3-11. Comparison of light transmission of dry coated vs uncoated glass.

Figure 3-12 shows transmission measurements under steam condition where both coated and uncoated glass slides were subjected to steam from boiling water. As shown, uncoated glass slide became ‘foggy’ due to condensation and transmission drops significantly an average value of around 65%. The coated glass slide, on the other hand, retained its transparency under the steam condition. It is worth noting that the transmission through ‘foggy’ coated sample is even better than that through dry coated sample across the whole measured spectrum of wavelengths, as can be seen in Figure 3-12. The average increase in transmission amounted to approximately 1.2% and can be possibly attributed to a thin film of liquid water forming on the glass surface, acting as an antireflective coating.

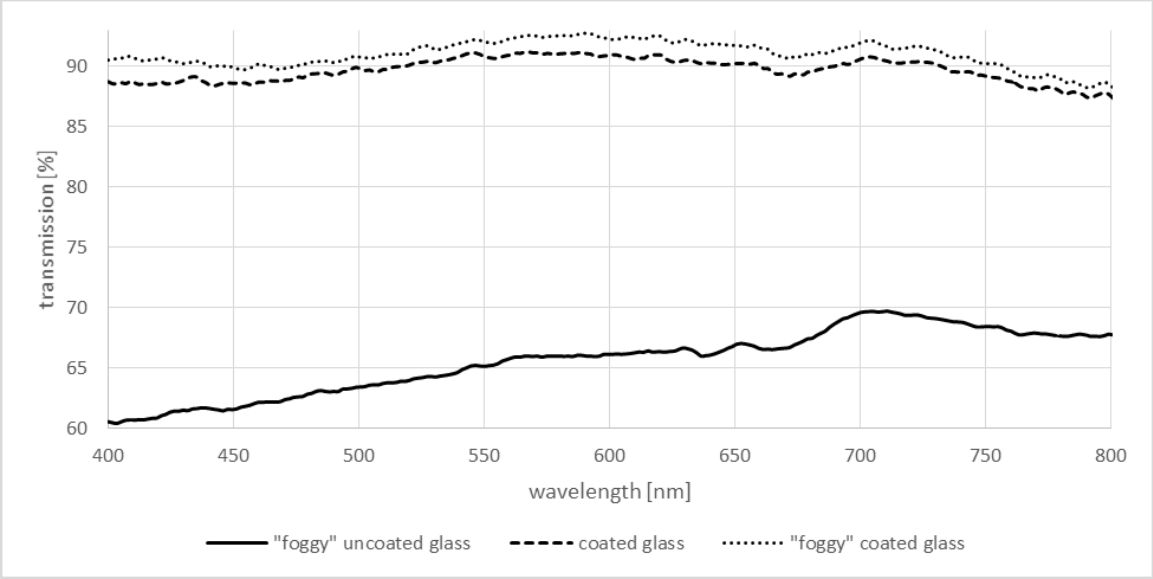

Figure 3-12. Comparison of light transmission of coated vs uncoated glass with condensation.

3.5 Conclusion

Silver nanoparticles of ~15nm in diameter were successfully synthesized and coated onto a glass substrate. The coating technique involved the use of a dual regime coating apparatus, which allows for fine coating thickness control and layer uniformity. Through precise droplet velocity control, the system facilitates near ideal droplet impact conditions at the surface, minimizing the chance of clogging/condensation inside the nozzle. Furthermore, focusing effect of the nozzle produces much less waste as most droplets are deposited onto the surface having the velocity falling into the “spreading regime” window. The coating produced exhibited strong superhydrophilic properties with water contact angles of around 6 degrees, as well as is shown to possess antifogging properties. In addition, coated samples showed a slight improvement in light transmission in the visible spectrum with the average increase of approximately 0.7% in dry state and nearly 25% in foggy state. The unique combination of antibacterial properties of silver

nanoparticles, together with superhydrophilic and antireflective behavior of the produced coating may potentially benefit numerous areas of research and industry, particularly in the biomedical sector.

Chapter 4 **Development and Evaluation of Flame Assisted Dual Velocity Nanoparticle Coating**

This paper was presented at the 11th International Conference on Micro Manufacturing (ICOMM 2016) and its extended version accepted for publication in ASME Journal of Micro- and Nano-Manufacturing in 2017.

Maxym Rukosuyev, Syed Baqar, and Martin Jun." Development and Evaluation of Flame Assisted Dual Velocity Nanoparticle Coating System", ASME Journal of Micro- and Nano-Manufacturing (2017)

This chapter provides the overview of the next step in the development of the coating system introduced in earlier chapters. The main goal of this chapter is to demonstrate the potential for material processing at elevated temperatures using a novel design of a torch-like device incorporated into the existing nozzle body. Furthermore, some properties of the resultant silver nanoparticle coating are also studied.

Contributors:

Maxym Rukosuyev – designed, manufactured, tested the flame assisted coating system, and completed the manuscript.

Syed Baqar – helped in conducting the experiments, data recording, and SEM imaging.

ABSTRACT

The importance of coatings in modern science and industry is great and the system presented in this manuscript attempts to provide a method of creating high quality nanoparticle coatings with *in situ* sintering of nanoparticles. Dual regime nozzle creates close to optimum conditions for particle delivery and deposition and the addition of *in situ* thermally assisted coating makes it more productive. Preliminary results show systems uniform coating and in situ sintering capability.

4.1 Introduction

Coatings today are widely used throughout industry as well as research in electronics, optics, biomedical experiments etc. [2-4]. Aside from the properties of the material used for coating, coating properties will, among other things, will differ strongly depending on the method of the application and the equipment used. The need for large area as well as micro scale coating led to the development of various spray coating techniques. Size consistency of the aerosol droplets, their actual diameter, and the droplet velocity are two parameters that largely determine the final quality of the coating layer. Ultrasonic atomization is known to work with a variety of materials as well as to deliver consistent droplet size for a particular liquid (usually order of 1μm -10μm) [69]. Companies like Sonaer, Sono-Tek, Optomec, and several others are using piezo based nebulizers in their microprinting and coating devices. Unlike Sono-Tek, Optomec utilizes a separate chamber to produce aerosol droplets. Therefore, the vibration frequency used in the atomizer can be higher which results in smaller droplet size. Optomec's nozzle is developed for microprinting and uses "shroud air" to focus and accelerate the droplets, and is not suitable for coatings on larger scale. Aerosol is pushed through a narrow channel, which can potentially clog the exit hole.

Once applied onto the surface, many coatings require post curing or sintering to provide better adhesion and remove any polymer nanoparticle encapsulation [25]. There are several methods to achieve *in situ* sintering and thermal treatment of coatings used by researchers today. Commercially available oxyacetylene flame spray torch (FST) was successfully used to produce bioactive composite coatings of titanium alloy and bioactive glass [70] and protective coating on stainless steel [71]. However, in case a

contamination free coating needs to be produced, the use of hydrocarbon fuel mixtures (commonly used in FST-type devices) is better to be avoided. When higher temperatures are required such as in case of refractory metals deposition, plasma spray deposition (PSD) techniques are used [72, 73]. These are quite expensive and require the use of highly specialised equipment. In lower temperature applications such as polymer thermal treatment, a simple diffusion flame torch can also be used [74-76]. In some cases, the hydrocarbons contained in the fuel form the functional coating [77]. Suspension thermal spraying has also been done using modified commercially available high-velocity oxyfuel gun [78].

Furthermore, some coating techniques use pyrolysis to facilitate the formation of the coating material from a precursor solution [26].

The goal of the present research was to design a spray coating device which would overcome some of the limitations of the existing coating solutions. Ultrasonic droplet generation was chosen as the most reliable mean of producing consistently sized small diameter droplets. Large outlet of the deposition nozzle ensures no clogging occurs during the coating process. At the same time, high speed central gas jet would focus and accelerate droplets to close to optimum velocities for efficient deposition. In addition, a deposition nozzle that incorporates a torch-like device was also developed. This system provides the opportunity to attempt an *in situ* sintering of the applied coating and/or encapsulating polymer removal. That allows to avoid time consuming and sometimes difficult to perform on large areas sintering/curing step. The axisymmetric geometry of the nozzle ensures circular cross section of the exit jet unlike the techniques where the particles are injected into the flame at an angle [79]. Furthermore, the pyrolysis process

can now be performed in a single step with the coating application, which would greatly reduce the effort of producing advanced coatings from precursor solutions.

4.2 Particle impact dynamics

A droplet impacting hard surface, depending on the conditions, will either rebound from the surface, splash off the surface subsequently re-entering the airstream, or spread and adhere to the surface. For best coating results, it is required for the particles to spread and form a thin film, thus ensuring the maximum amount of material is retained on the surface. A dimensionless number K_m is used to give an estimate of droplet behaviour upon the impact.

$$\mathrm{K_m} = \left(O_h{}^{-2/5} * \mathrm{We}\right)^{5/8}$$

Where

$$O_h = \frac{\mu}{\sqrt{\mathrm{T} * \rho * \mathrm{D_m}}}$$

Where

$\boldsymbol{\mu}$ liquid's dynamic viscosity and $\boldsymbol{O_h}$ is the Ohnesorge number.

The droplet does not enter the splashing regime unless K_m is greater than the critical K_{mc} value (K_{mc}=57.7) [32]. To minimize droplet adhesion to the internal surfaces of the coating system conduits, a rebounding regime should be established before nozzle's exit. The Weber number gives a guideline for establishing a non-stick condition inside the system.

$$We = \frac{w_0^2 D_m \rho}{T}$$

Where

Dm average droplet diameter,

T surface tension,

ρ density,

w_0 velocity normal to the surface.

Rebounding regime is established for $We<10$ [41].

For the coating process to proceed uninterrupted with no large droplets forming inside the system, and maintain close to ideal droplet velocity at the impact, a dual-velocity nozzle setup is needed. Lower droplet velocities are necessary to avoid condensation on the system's internal surfaces, whereas higher velocity is desirable at the nozzle's exit to allow for the best possible deposition regime with best adhesion and minimal waste of material.

4.3 Design

To ensure that the dual-velocity requirement is met, one of the design objectives is to decouple the production of atomized droplets and their deposition. Therefore, the ultrasonic atomizer and the deposition nozzle are two separate units.

Atomized droplets are transported from the ultrasonic nebulizer to the deposition nozzle by the slow moving carrier gas flow. The tube located at the central axis of the nozzle accelerates and focuses the particle stream. An addition of flow conditioning unit ensures that the flow is axisymmetric, free of turbulence, and that the larger sized droplets are separated from the main flow and drained out of the system (Figure 4-1).

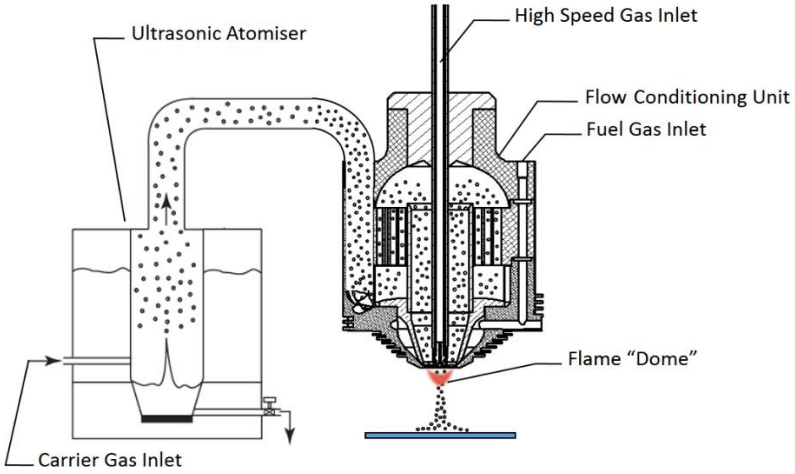

Figure 4-1. System schematics.

Flow conditioning unit (FCU) is an intermediate device that is placed between the nozzle and the atomizer. Asymmetric droplet inlet and a built in honeycomb structure allow only the smaller and lighter droplets to travel to the nozzle's exit.

Figure 4-2 shows the droplet jet coming from the nozzle's exit. The dome-like shape is caused by a circular stable vortices formed by the slower droplet carrying gas entrained by the higher speed central jet. The character and the size of the "dome" is dependent on the position of the central tube with respect to the edge of the nozzle's exit and the corresponding velocities of the slow and fast moving gas streams.

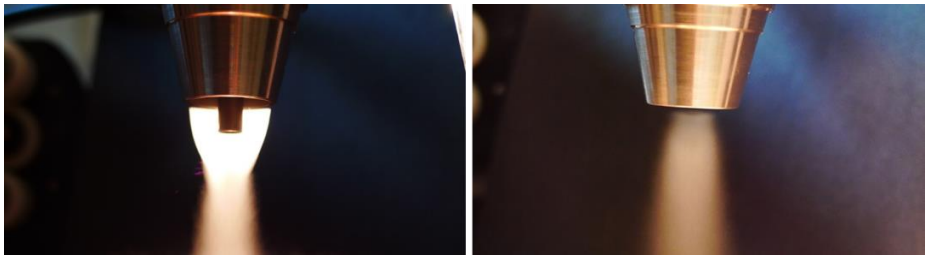

Figure 4-2. Images of the particle jet exiting the nozzle with variable center tube location

4.3.1 Flame assisted coating

When coating the surface with fine particles, it is important to insure good uniformity of the coated layer as well as adhesion to the coated surface and between particles. While the former is primarily a function of the coating system, the latter can be accomplished in several different ways.

In some cases, after the application of the coating material the layer needs to be cured/dried at certain temperature depending on the coating material. This method will ensure adhesion between particles and material and, in some cases, fuse/sinter the particles together to form a uniform layer of material on the substrate. However, this method requires additional step in coating process, subjects the substrate to high temperature for a prolonged period of time, and requires additional piece of equipment (oven).

To avoid the extra step of post-curing material being applied, plasma coating can be used. Plasma coating ensures that coating material, usually in the form of powder or slurry, melts before it reaches the substrate surface. It is done by passing a stream of material through high temperature (up to 10000 ^{o}K) plasma which is, essentially, a high voltage arc discharge. Subsequently, molten material contacts the substrate surface and, if rapidly cooled on contact, reaches temperatures below melting point, thus forming a coating layer. Taking into account the complicated nature of the high voltage equipment, cooling facilities, price of the electrodes and other expendables, this method can be quite costly and will require specialized facilities and trained personnel.

System presented in this paper, does not require the expenditures associated with plasma coating and, at the same time, provides a method of “one step” coating and

curing/sintering. Figure 4-3 shows the overall schematics of the Circular Flame-Assisted Coating Nozzle (further CFACN).

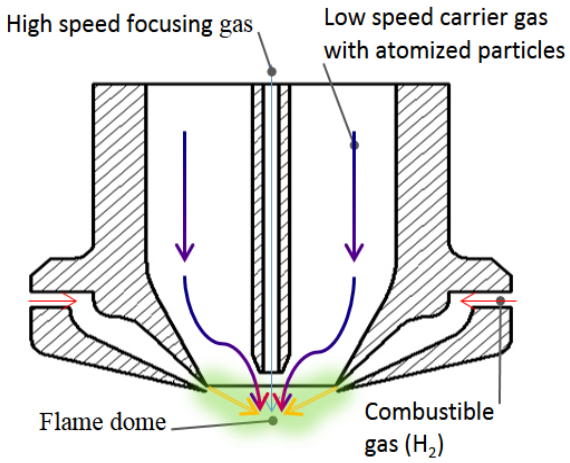

Figure 4-3. Gas flow schematic.

The working principle of the nozzle is based on the previous design of the center air nozzle used for nanoparticle coating. The center high speed gas jet serves the purpose of focusing and accelerating the stream of particles. Combustible gas or gas mixture is fed through a narrow channel surrounding the nozzle exit. The combined effect of the center high speed gas and the ignited gas mixture surrounding the nozzle exit creates a "dome of flame" that the particles will travel through. The temperature of the flame will depend upon the gas mixture used. In the case of hydrogen, its flame temperature is around 2000^{o}C when burned in air. The transition time through the flame can be adjusted by regulating the carrier gas and center gas velocities.

The image of a working prototype of the nozzle is shown in Figure 4-4. The formation of the dome can be clearly seen at the exit of the nozzle. The orange glow of the flame is caused by the injection of polymer coated silver nanoparticles. The temperature of the

nozzle remains comparatively low as can be seen in Figure 4-4. The air stream passing through the larger diameter tube carrying the particles adds to the cooling effect so that the nozzle tip remains “warm” to the touch.

Figure 4-4. Low temperature demo on the nozzle.

As a ‘proof of concept’, the nozzle was tested with polymer encapsulated silver nanoparticles. To achieve the goal of uniformly distributing the particles over the substrate’s surface, a preliminary set of experiments with the torch off were carried out to establish appropriate distance from the tip of the nozzle to the coated substrate. The nozzle tips with 15mm diameter exit orifice showed best results while being positioned approximately 30mm - 35mm from the substrate. The distance between the nozzle and the substrate, in combination with the appropriate motion velocity of the nozzle across the coated piece, ensures rapid evaporation (1sec – 2sec after deposition) of the solvent and therefore, absence of particle agglomeration. Smaller droplets do not have enough time and spaced sufficiently far apart to not coalesce thus preventing individual nanoparticles to form larger groups. Subsequently, several experiments were performed with the torch active. Some of the results of the above mentioned experiments are shown in the subsequent section.

4.4 Results

The results shown below illustrate the proof of concept and the potential capability of the system to be used in various applications. Two substrates (aluminium SEM stub, and a glass microscope slide) were chosen to conduct the initial tests of the system. The particles, were polymer encapsulated silver nanoparticles (Vive Nano inc., and in-house synthesized Ag nanoparticles with mean diameter of ~25nm) suspended in water. Droplets were produced using an ultrasonic atomizer (f = 3MHz, P = 15W). Air was used as a carrier gas and hydrogen as combustible agent. The use of hydrogen ensured absence of possible carbon deposition on the substrate or coating layer, which could occur in case some sort of hydrocarbon gas is used as a source of heat. Spray coating was conducted with ~66 in/min horizontal velocity at a distance of ~25 mm from the coated surface to the tip of nozzle.

4.4.1 Polymer removal and in situ sintering

Figure 4-5 and Figure 4-6 show images of coated glass and aluminium samples respectively, comparing ‘flamed’/cold’ side by side. As can be seen in images below, ‘cold’ samples exhibit a light brown colour whereas in case of heated samples, the colour is grey/dark grey, which indicates that the flamed samples have had the polymer coating burned off.

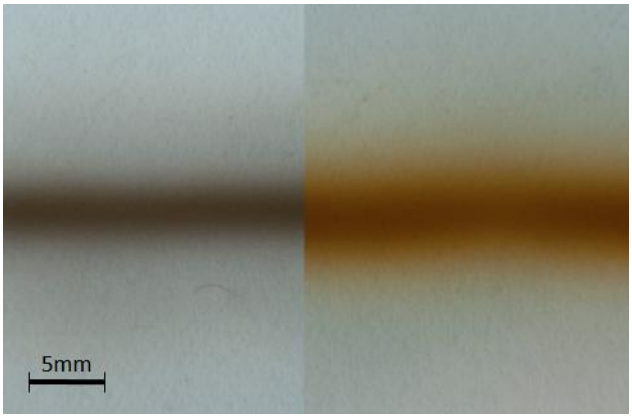

Figure 4-5. Coating on glass ('flamed' left, 'cold' right).

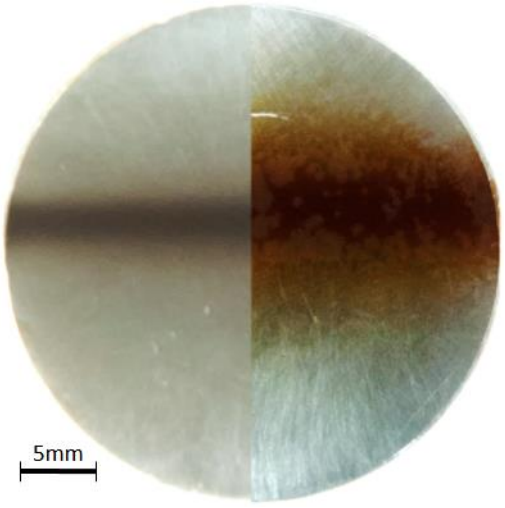

Figure 4-6.Coating on aluminum ('flamed' left, 'cold' right).

Subsequently, a series of SEM images of the ‘flamed’ and ‘cold’ aluminium samples were taken. As shown in Figure 4-7, the polymer encapsulated silver particles form a coating with flake-like appearance. Figure 4-8 illustrates that the particles are fused together on the top of the layer and form a coherent lattice deeper and closer to the substrate. That proves the assumption that the temperature achieved and the transition time is sufficient to burn off polymer and soften the outer skin of silver particles. Since the temperature setting has not yet been tuned perfectly, some agglomeration in the resulting coating has been observed.

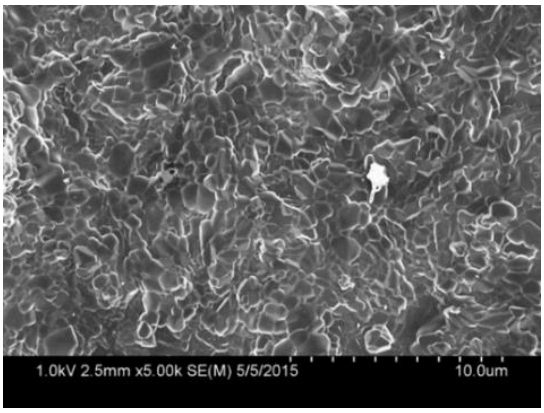

Figure 4-7. 'Cold' sample at 5000X magnification.

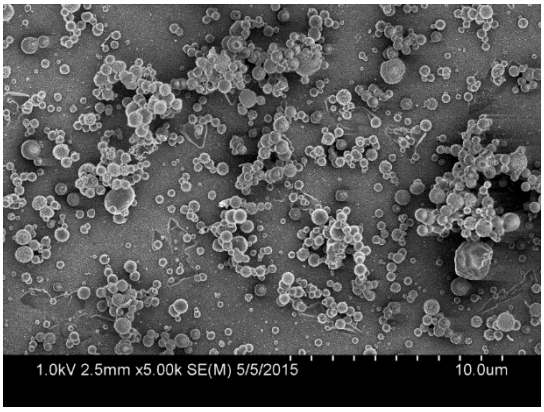

Figure 4-8.'Flamed' sample at 5000X magnification.

4.4.2 Coating on polymer

Another possible application of the flame assisted coating system is the surface modification of polymer substrates. Surface modification of a polymer using a one-step process can have numerous effects on the interaction of the coated part with the environment. To examine the effect of the nanoparticle impregnation on the performance of PTFE based polymer, an attempt was made to coat it with silver encapsulated nanoparticles. Figure 4-9 and Figure 4-10 show the surface of the sample before and after it has been treated with silver nanoparticles using the flame-assisted coating technique.

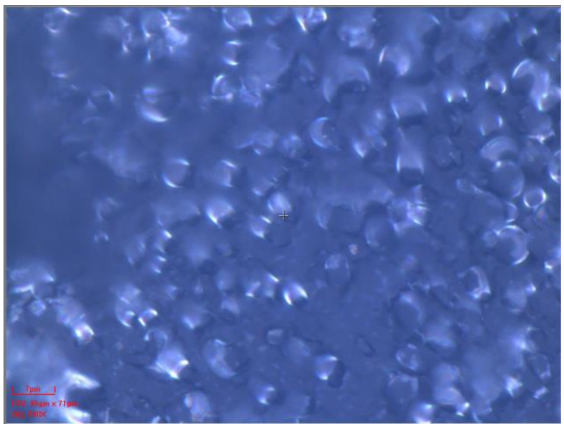

Figure 4-9. Teflon surface before treatment (optical microscope image using 100X magnification objective lens).

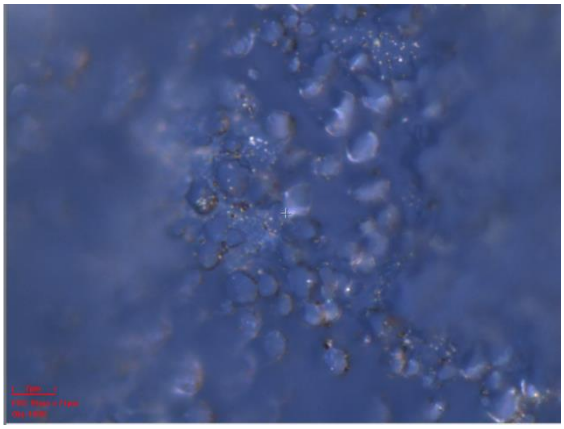

Figure 4-10. Teflon surface after treatment (optical microscope image using 100X magnification objective lens).

PTFE is known to be intrinsically hydrophobic. The nanoparticle treatment has apparently increased the hydrophobicity of the bare base material even when the surface has been rubbed repeatedly. The water surface contact angle measurements were performed on both samples using 10µl droplets of deionized water with a goniometer (Holmarc HO-IAD-CAM-01B). Average water contact angles recorded for untreated

versus coated surface were 90.7 degrees as shown in Figure 11 and 94.2 degrees as shown in Figure 12, respectively.

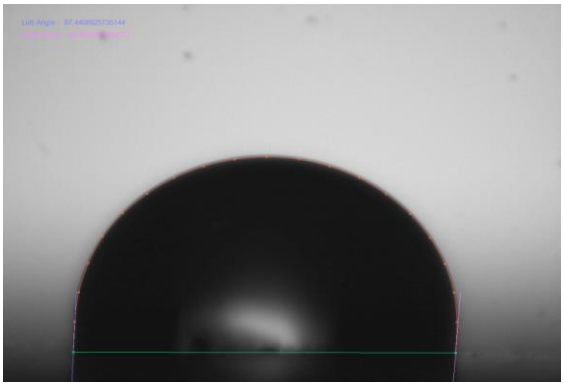

Figure 4-11. CA measurement on base Teflon.

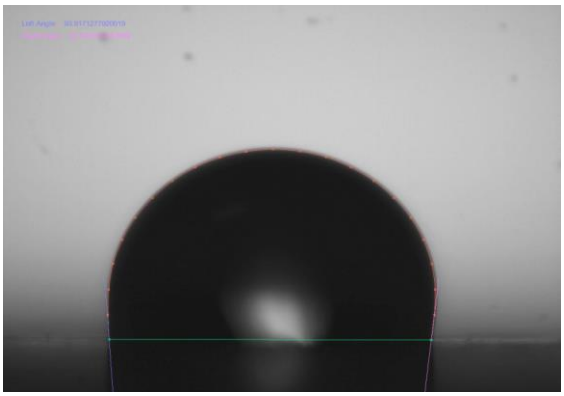

Figure 4-12. CA measurement on nanoparticle treated surface.

4.4.3 Antireflective/superhydrophilic coating on glass

Ten coating cycles were performed on microscope glass slide, after cleaning it thoroughly with ethyl alcohol. The contact angle (CA) measurement (with water) on surfaces treated with flame assistance showed rapid reduction to below 10 degrees within only 50 milliseconds, thus indicating that the surface has become superhydrophilic. The contact angle continued to drop and was measured to be about 7 degrees at ~900 milliseconds after deposition.

A comparison of CA readings on a glass slide coated in “cold” and flame assisted regime is shown in Figure 4-13. CA comparison of “hot” and “cold” coated glass samples.. In “cold” case, the CA of the droplet measured on coated surface took about 2 seconds to drop below 10 degrees and continued to drop down to ~6 degrees.

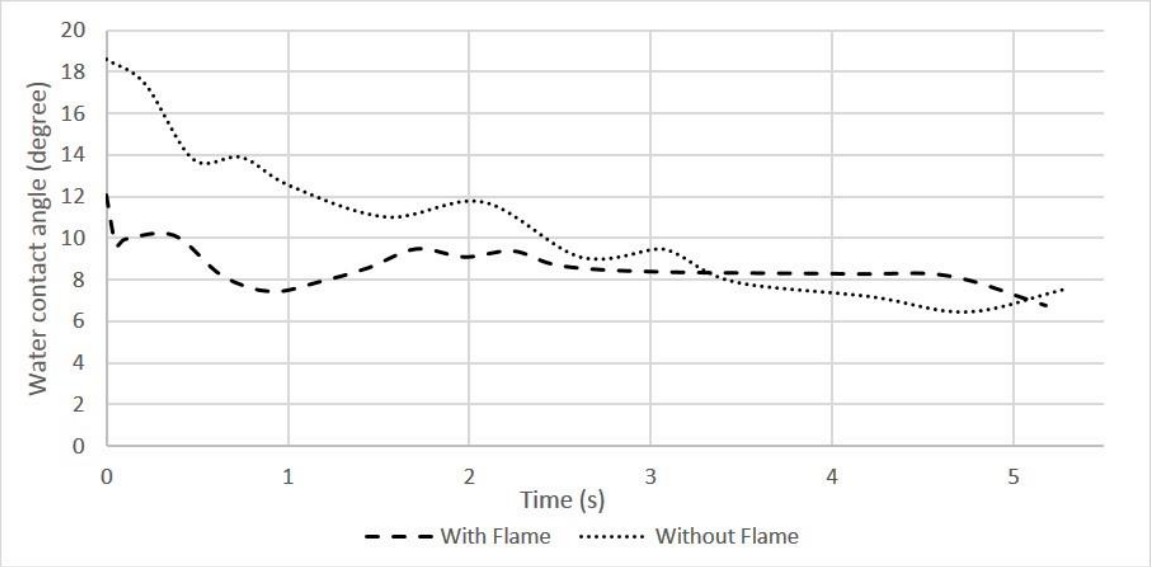

Figure 4-13. CA comparison of “hot” and “cold” coated glass samples.

The ability of coated samples to transmit/reflect light was tested in dry environment as well as when exposed to water vapor. Light transmission results were compared against those obtained from untreated glass samples. The light transmission measurements were taken using SR300RT reflectometer (Angstrom Sun Technologies). Figure 4-14 illustrates the differences in light transmission between coated and uncoated glass slides in the visible spectral range. As can be seen, both cold coated and flame coated surface exhibit better light transmission in the visible part of the spectrum. Furthermore, flame coated samples have markedly better transmission at shorter wavelengths (400nm-600nm) than both cold coated and uncoated samples.

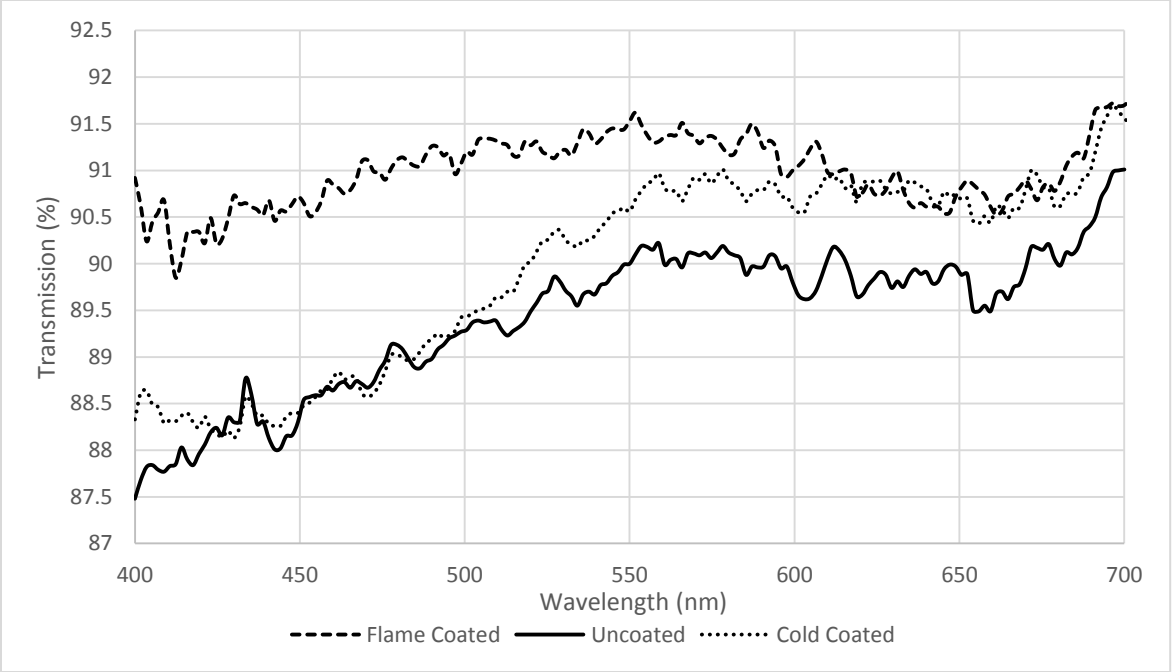

Figure 4-14. Light transmission for coated and uncoated glass samples.

4.5 Conclusions

The coating system described above realizes a dual velocity regime to ensure close to optimum conditions both inside the nozzle and at the substrate surface. Additionally, built in ring flame jet allows to heat the particles passing through nozzle's exit. This combination can provide an advantage of single step coating with minimal post processing. In-situ sintering using the ring flame has been demonstrated. The coating system has been used to coat surfaces with nanoparticles to improve hydrophilic properties of the surface. Further exploring of the capabilities of the system will allow to find new applications and improve system's performance.

Chapter 5 **Flame Assisted Spray Pyrolysis Using Annular Flame Nozzle with Decoupled Velocity Control.**

This paper was presented at the World Congress on Micro and Nano Manufacturing (WCMNM 2017) and its extended version (in this dissertation) is being prepared for submission in Journal of Coatings Technology and Research.

Maxym Rukosuyev, Syed Baqar, and Martin Jun. "Flame Assisted Spray Pyrolysis Using Annular Flame Nozzle with Decoupled Velocity Control", submitted for publication to the Journal of Coatings Technology and Research (2017).

This chapter introduces a novel flame spray pyrolysis device that allow nanoparticles to be synthesized and deposited in a single step coating cycle. Similar device has been used in experiments described in the previous chapter and therefore is a continuation of the same line of research. The scope of this paper is confined to the introduction of the device itself, basic principles of the pyrolysis process, and preliminary results obtained in the synthesis of silver nanoparticles.

Contributors:

Maxym Rukosuyev – designed, manufactured, tested the flame spray pyrolysis system, and completed the manuscript.

Syed Baqar – helped in conducting the experiments, data recording, and SEM imaging.

5.1 Introduction

Flame Spray Pyrolysis is a promising and adaptable [80] technology which is in use by several giants in chemical industry including DuPont, Ishihara, and Degussa for the synthesis of metals, metal oxides, catalysts and functionalized nano sized particles. Some of the examples include carbon black, carbon nanotubes, Ni, Pd, Pt, Ag, Au, Ti, TiN, TiB2, SiO2, TiO2, Al2O3, CeO2, In2O3, WO3, Co3O4, CuO, ITO, ZrO2 and SnO2 [81-84] to name a few. Depending upon precursor delivery method, it can be classified into

vapor-fed aerosol flame synthesis, flame spray pyrolysis and flame assisted spray pyrolysis [85, 86]. In flame assisted spray pyrolysis, a precursor is usually based on aqueous solution and cannot sustain the initial flame, whereas in flame spray pyrolysis the precursor is mixed with fuel. Thin film deposition using flame spray pyrolysis uses a substrate instead of a particle collector usually made of PTFE or glass fiber based filter [87].

In general, spray pyrolysis setup consist of a device for generation of small droplets (spray) of precursor solution, carrier mechanism, high temperature treatment setup, and a particle collector. The use of an ultrasonic atomizer keeps the spray generation mechanism separate and provides consistently sized droplets with the delivery rate controlled by the carrier gas flow. The empirical formula for estimating mean droplet diameter is [40]:

$$D_p = 0.34\left(\frac{8\pi\sigma}{\rho f^2}\right)^{\frac{1}{3}}$$

where, D_p is the droplet diameter, σ is the liquid surface tension, ρ is the liquid density, and f is the atomizer frequency. Therefore, for given conditions droplet size can be varied by using atomizing transducer with different specifications (resonant frequency and power).

High temperature treatment of the precursor droplets can take many forms. These include the use of a heated substrate [88], quench cooled reactor [89-93], diffusion flames where fuel, oxidant, and aerosol made of precursor and carrier gas pass through separate concentric tubes [92], and spray flames where fuel and precursor are premixed and ignited [94]. Each of these techniques can take a different path of nanoparticles

generation and deposition on the substrate. In this work, a variant of diffusion flame spray pyrolysis was used to generate and deposit nanoparticles in a thin film, which can be used in numerous applications including sensors fabrication, coatings, fuel cell electrodes etc. This method is essentially a solution based chemical deposition process having distinct advantages of being simple, fast, less expensive and applicable for coating large area substrates. The waste products are usually water vapors and carbon dioxide [82].

Flame spray pyrolysis has additional advantage over the other spray pyrolysis methods in that it is generally a single step process and does not require additional annealing step which is required in conventional spray pyrolysis or wet chemistry methods [81]. It has also been demonstrated for continuous roll-to-roll deposition of nanoparticles. [95]

The mechanism of nanoparticle formation and its subsequent deposition is described differently by different authors. It is admitted by most researchers that the mechanism is not very well understood [96-98] and cannot easily be generalized, since it is found to be dependent on varying parameters for different precursors as well as reactor configuration. Pratsinis [97] noted that since the principle of continuum do not hold for nanoparticles and the bulk material properties change at that scale and attributed the present knowledge to be largely based on simulations and experimental results.

Nanoparticle formation is strongly dependent on the precursor and other spray pyrolysis parameters, not limited to those explained below. Different researchers [99-106] have explained varying routes of nanoparticle formation for different precursors. Cho et al. [99] prepared silica nanoparticles from TEOS as well as silicic acid, explained that particles formation takes one of three routes (A, B, or C). Selection of the route

depends on the spray pyrolysis parameters, especially flame temperature. This explanation, although may not be applicable for all precursors, can still serve to gain understanding of particle formation mechanism.

In case ‘A’, the reaction starts and completes in vapor phase. This is applicable when the evaporation time of the precursor droplets (which depends on flame temperature, concentration of precursor, etc.) is shorter than time to form particles. Lower concentration of precursor and higher flame temperature favors this route. Since the particles form quickly, they start to form aggregates after nucleation, en route to the substrate. In case ‘C’, the evaporation time of the precursor droplets is longer than time to form particles. In this case, small seed particles start to form within the precursor droplet due to precipitation. They grow within the droplet by condensation and coalescence to form larger particles, while the precursor droplet completes its evaporation. Higher concentration of precursor and lower flame temperature are reasons behind this route. In case ‘B’, the evaporation time of precursor and particle formation time are comparable, so a combination of routes ‘A’ and ‘C’ can be expected to take place.

A number of parameters have been known to influence the geometry of generated nanoparticles. Increasing the nozzle feed rate (the speed at which it is traversing over the substrate) reduces the amount of precursor that is being processed per unit area which results in fewer deposited nanoparticles. If it is coupled with high flow rate of precursor/carrier gas, it can lead to shorter residence times and reduced nanoparticle production. Increasing the flow rate of carrier/dispersant gas reduce the concentration of spray in flame, its residence time in the flame and also the flame temperature. This generally leads to smaller size of particles [101, 107]. Increase in the distance between

burner/nozzle edge and substrate decreases the number of nanoparticles deposited on the surface. Since the nanoparticles have to pass through the layer of air above the substrate in which the particle transport mechanisms of diffusion and thermophoresis are happening; and with increased distance, the gradients of particle content and temperature decrease, causing fewer particles to transport through the layer [82].

Temperatures of reaction space and substrate plays major part in the resultant coating. If substrate temperature is elevated, either by flame or by external means, it leads to formation of dense films [81]. Flame is generated by burning a fuel (e.g. hydrogen, methane, propane, acetylene etc.) with an oxidant (e.g. oxygen, air). The flame temperature is primarily controlled by stoichiometric ratio of fuel and oxidant. Choice of fuel is also important, as it can introduce impurities into the film (e.g. use of acetylene at higher temperature can produce carbides [108]). Hydrogen-air flame can reach up to 2200°C, but it is low for small stoichiometric ratios. Higher jet velocity leads to shorter residence time, which means that droplets would have less time to evaporate and hence leads to smaller particles. The increase in flame temperature reduces the evaporation time and hence can promote smaller particle formation, but if increased too much would result in aggregates to form [101].

$AgNO_3$ is known to produce silver particles upon thermal decomposition:

$$2AgNO_3\ (s) \rightarrow 2Ag\ (s) + O_2\ (g) + 2NO_2\ (g)$$

Pluym et al. [109] produced micron sized silver nanoparticles using spray pyrolysis. Pingali et al. [110] and Mäkela et al. [111] produced particles with size in the order of

tens of nanometers using spray pyrolysis (tube furnace) and flame spray pyrolysis, respectively.

Research presented in this manuscript, introduces a new nozzle design for the production of nanoparticles through spray pyrolysis and their subsequent deposition. The design features of the nozzle allow for a wide range of adjustment in particles flow pattern and velocity, temperature, and focusing/defocusing of the jet on the substrate. The nozzle can be used with any atomiser available. Ultrasonic nebulizer was used as it is relatively easy to maintain consistent droplet size of aqueous precursor solution.

5.2 Experimental setup

The basic principle of operation of the dual velocity deposition nozzle is described elsewhere [112]. To facilitate the flame spray pyrolysis process, a fuel injection setup was added to the basic design of the nozzle. The schematic of the updated nozzle design is shown in Figure 5-1.

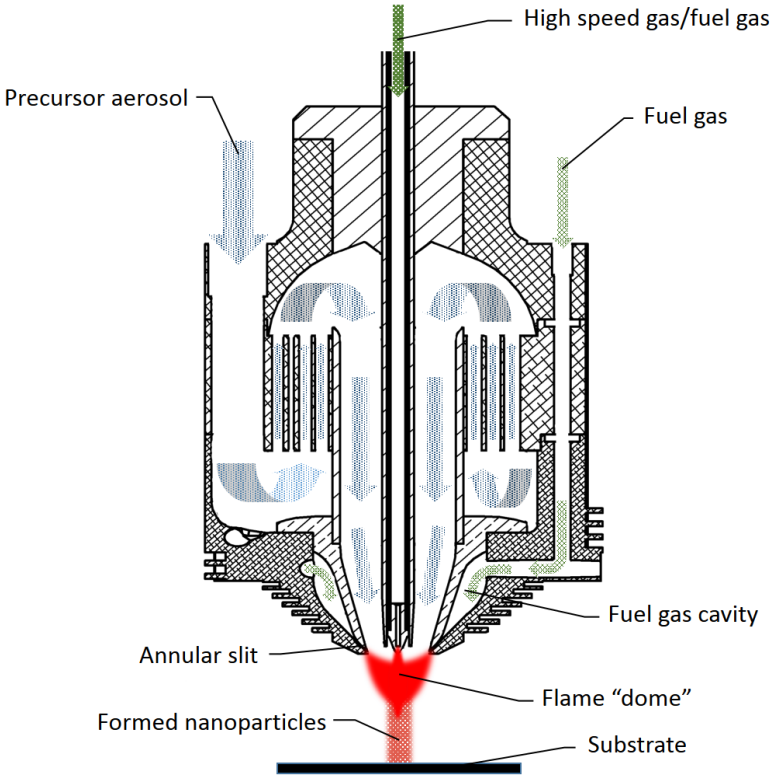

Figure 5-1. Dual velocity nozzle with added fuel injection.

The new nozzle design incorporates inner funnel piece at the nozzle exit which, together with the outer wall of the nozzle, form the fuel gas cavity and a narrow annular slit. Fuel gas (hydrogen in this case) is supplied through the said circular slit and mixed with oxidizer (air/oxygen) at the nozzle exit. The oxidizer is fed through the tube located in the center of the nozzle as well as by the carrier gas flow. Central tube is double-walled, which allows additional fuel gas delivery to the center of the nozzle exit for added temperature control. The aerosol enters the nozzle from two sides (only one shown in Figure 5-1) and begins circular motion in the lower section. Due to cyclone effect, larger droplets settle on the walls of the lower chamber and do not enter the honeycomb mid-section. Passing through honeycomb, the turbulence of the flow is greatly reduced and the emerging flow is close to axisymmetric. To ensure a "non-stick" condition, the

velocity of the aerosol is kept in 6m/s-10m/s range. Once the droplets approach the exit of the nozzle, they are forced to the middle of the cross section by the nozzle's geometry and a drop in static pressure due to higher velocity of the gas coming from the central tube. Coming through the flame, the process of precursor decomposition and nanoparticle formation begins. Subsequently, nanoparticles can be either deposited on the spot, or collected for further processing. Due to the axisymmetrical nature of the gas flow through the nozzle, the particles can be deposited in a well-controlled and uniform manner ensuring high degree of control over coating layer thickness. Since the processing of the precursor solution starts when it is already in the aerosol form, other nanoparticles that are already in suspension and atomized with another devise can be added, thus the production of a composite coating is possible.

The overall system schematic of the system is shown in Figure 5-2. Flow control valves allow for fine control of fuel/air mixture, which is crucial for maintaining the optimum temperature for the decomposition reaction to take place. Mass flow meters (Hastings Teledyne HFM-200) are used to determine the amount of hydrogen and air in the mixture.

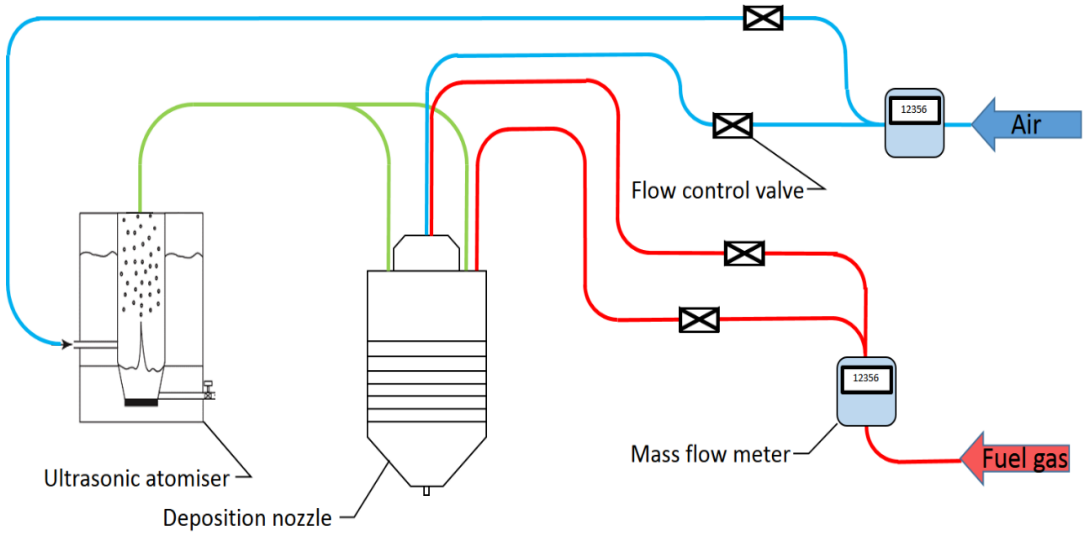

Figure 5-2. Overall system schematics.

The nozzle was mounted onto a CNC router (Romaxx CNC Systems) to facilitate the coating process (Figure 5-3). CNC router ensures consistent coating application with set overlap, feed rate, and distance from the nozzle tip to the surface to be coated. The resonant frequency and power of ultrasonic atomizing transducer was 2.4/3MHz and 12W respectively with output flow rate of ~ 400ml/hr. However the actual flow rate of mist carried out of the atomizer is controlled by carrier gas flow.

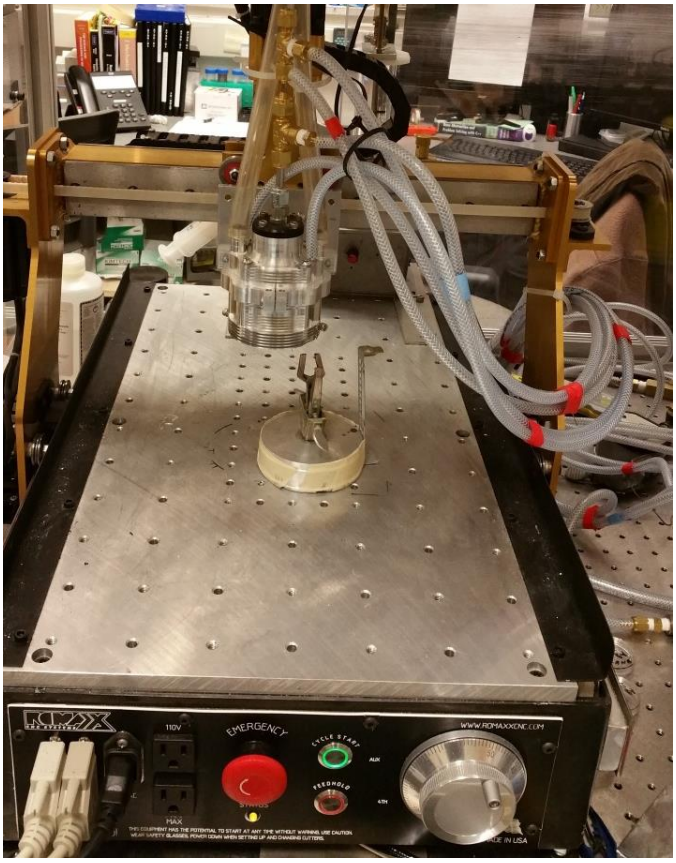

Figure 5-3. Nozzle mounted onto a CNC router.

Three sets of experiments were carried out to gauge systems performance and to validate its ability to produce and coat nanoparticles. 250 mg of silver nitrate ($AgNO_3$ >99%, Sigma Aldrich) was dissolved in 250 ml of deionized water to prepare stock precursor solution of 1 g/l under magnetic stirring for 25 min. It is known that $AgNO_3$ can produce silver ions in presence of light, which can lead to contaminant formation. Therefore, special care was taken to ensure that the whole experiment, including handling of $AgNO_3$ to preparing precursor solution, was conducted in the presence of as little light as possible and various parts of the flame spray coating setup were covered with aluminum foil.

For the first set, solution was diluted to 50mg/l, 100mg/l, and 200mg/l to see the effect of varying precursor concentration. Hydrogen gas was used as fuel and air as oxidant. In order to obtain the desired flame temperature (~780^{o}C measured by K-type thermocouple in the center of the flame "dome" and close to 550°C 22 mm from tip of the nozzle), the flowrate of air was kept at 480in^3/min, while that of hydrogen was 72in^3/min. Two resonant frequencies were used for the ultrasonic atomiser 2.4MHz and 3MHz in order to create the droplets of a slightly different size and see its influence on the resulting particle size. The experimental parameters and sample numbers are summarised in Table 5-1.

Table 5-1. Experimental parameters.

Sample #	Precursor concentration mg/l	Atomiser frequency MHz
1	50	3
2	100	3
3	200	3
4	50	2.4
5	100	2.4
6	200	2.4

The substrate was ultra-high vacuum (contamination free) aluminum foil (All –Foils Inc.) placed on an aluminum stub using conductive graphite paste (PELCO Conductive Graphite, Isopropanol base, Ted Pella Inc.). Before deposition process, the substrate was surface treated with Electro-technic's corona treater (BD-20). This treatment is known to help in increasing the bonding/adhesion to the surface by increasing its surface energy before coating. Spray coating was performed with 72 inches per minute of feed rate at a distance of 22 mm from the surface to the edge of nozzle. Second set of coating

experiments was conducted using the same substrate and substrate treatment, but the concentration was varied from 300mg/l to 100mg/l with temperatures set at ~780°C and subsequently increased to 830°C.

For the third experiment, precursor concentration was held at 100 mg/l. Microscope slide cleaned with ethanol was used as a substrate. Spray coating was performed with the same speed and distance from the substrate as in the first case. Spraying was carried out with an overlapping zigzag style facing operation on a surface area of about 1 in^2. The coating was observed to be optically transparent.

5.3 Experimental results and discussion

Three sets of results were obtained and analyzed. The first set of experiments provided insight into the nanoparticle size dependency on experimental parameters such as precursor concentration and aerosol droplet diameter. Second set illustrated particle size dependence on the flame temperature. The third experiment illustrated system's capability to produce a one-step functional coatings on challenging substrate such as glass.

5.3.1 Variable concentration and droplet diameter

Silver nanoparticles of average size ranging from 25nm to 40nm were successfully synthesized using the proposed nozzle design. Depending on the experimental parameters listed in Table 5-1, the average size of the particles will vary. A short summary of the average particle sizes is presented in Table 5-2.

Table 5-2. Average particle size for varying conditions.

Sample #	1	2	3	4	5	6
Average size [6]	40	37	33	28	27	25
Standard deviation [6]	10	9.5	6.5	10	5	5

Data presented in Table 5-2 looks somewhat counterintuitive as the largest nano particles are obtained from the droplets with the smallest diameter (3Mhz frequency atomizer produces smaller sized droplets than those produced by the 2.4MHz transducer). Similarly, lowest concentration of the precursor solution produced larger average particle size with highest standard deviation numbers. All other experimental conditions being the same, these phenomena could not be attributed to differences in temperature or the time it takes for the droplet to travel through the high temperature region as these were kept constant.

One possible explanation for the smaller size particles produced from droplets with larger diameter is the time it takes for the droplet to reach the temperature of the thermal decomposition of the precursor at which the nanoparticle formation occurs. Larger droplets will reach the decomposition temperature much later in the course of travel through the flame due to evaporative cooling of the droplet and poor thermal conductivity of water (precursor solution being water-based). In smaller droplets, on the other hand, the reaction will begin earlier and will continue for a longer period of time. Therefore, more of the precursor solution is converted into the nanoparticle resulting in its larger size.

Smaller measured size of particles observed in the experiments with higher precursor concentration is harder to explain. One possible reason for the larger apparent particle

size can be smaller particles agglomerating to form larger clusters in droplets with lower precursor concentration. Due to small size of individual particles, larger agglomerates can be easily mistaken for a single particle during measurement using SEM images, thus giving larger average recorded size. That can also explain larger standard deviation numbers observed in cases with lower precursor concentration.

Figure 5-4 shows an example of particle size distribution. In most cases, 80% of the particles are within 3nm of the average size with over 85% in case of larger droplet with higher concentration of precursor. It should be noted that the size of the particles is, among other things, governed by the size of the droplets produced by the atomiser. Since droplets exiting the atomiser range in size from approximately 3µm to 10µm (for 2.4MHz resonant frequency piezo), a narrower particle size distribution can be achieved if an additional droplet size sorting technique is utilised.

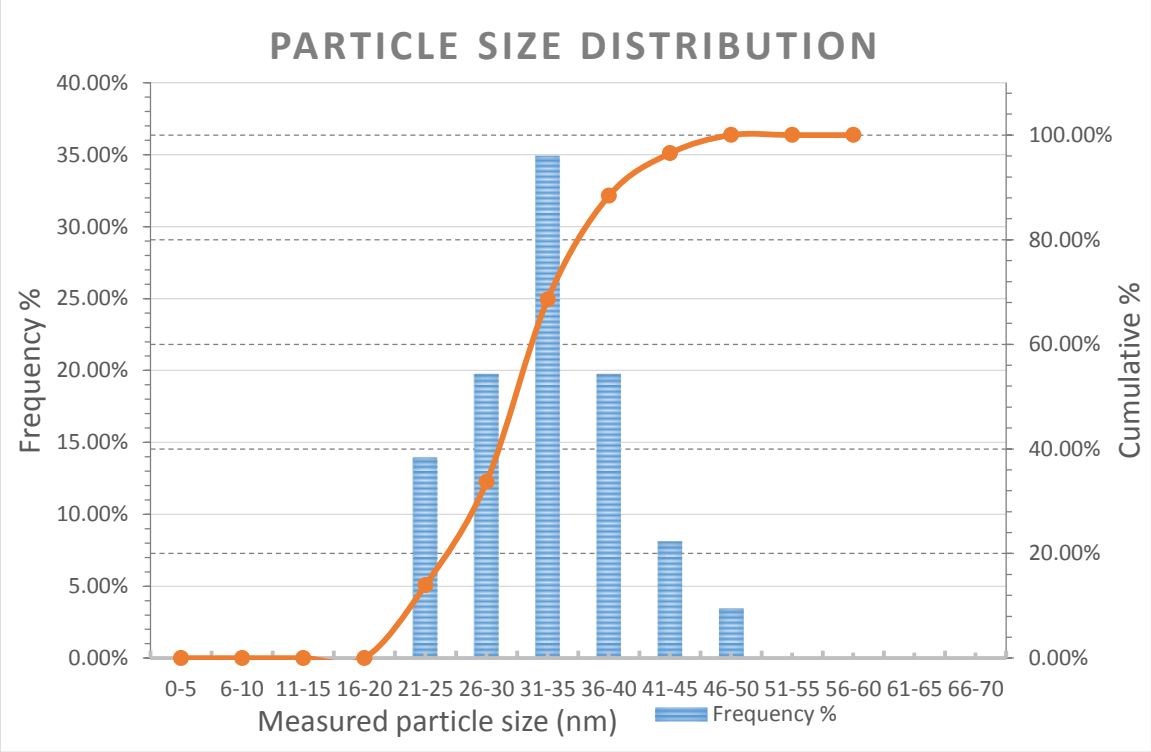

Figure 5-4. Particle size distribution for sample #3.

Sample SEM images of obtained nanoparticles are shown in Figure 5-5 and Figure 5-6. All specimens prepared for imaging were imaged in slow mode at 2 kV accelerating voltage and 10 μA current. The SEM images were taken at 5.1 mm working distance with 60% back scattering.

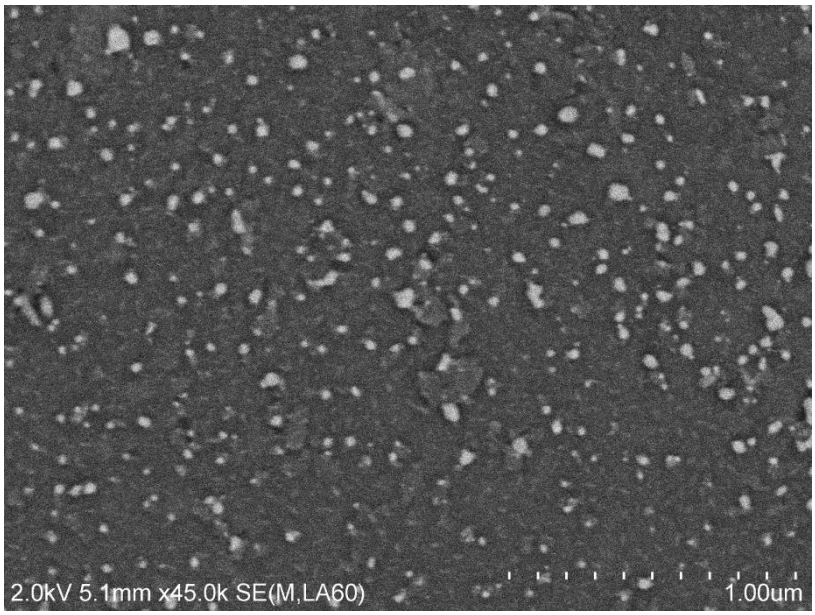

Figure 5-5. SEM image of sample #3 (concentration 200mg/l, frequency 3MHz).

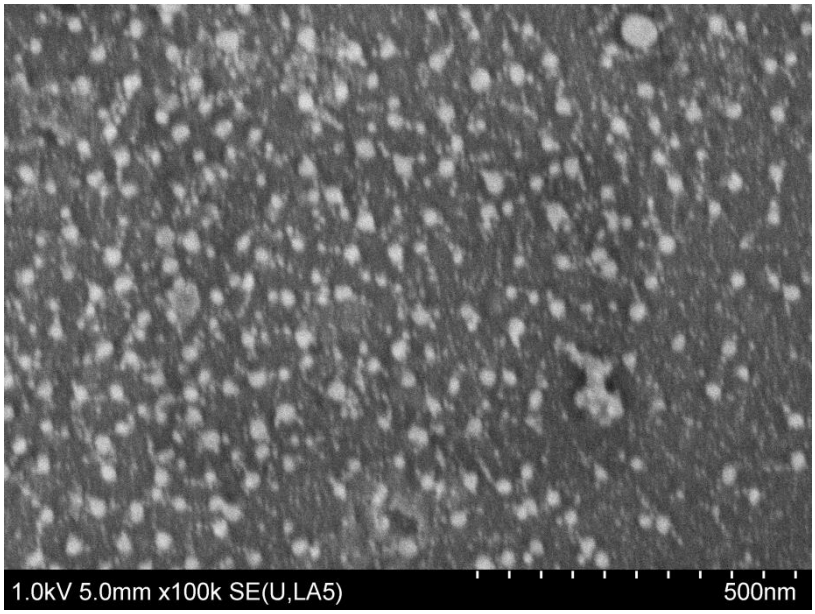

Figure 5-6. SEM image of sample #6 (concentration 200mg/l, frequency 2.4MHz).

In order to confirm that the bright spots observed in SEM images were silver nanoparticles, EDS (Energy Dispersive X-ray) analysis was performed using Bruker Quantex EDS system at 6 kV. The reason for selecting 6 kV was based on maximizing the L-line emissions, which for Silver requires a potential of 2.983 kV. Applying twice as much accelerating voltage maximizes emissions for better imaging. The spectrum maps (200,000X) in Figure 5-7 confirm that the bright particles in the SEM images are silver nanoparticles.

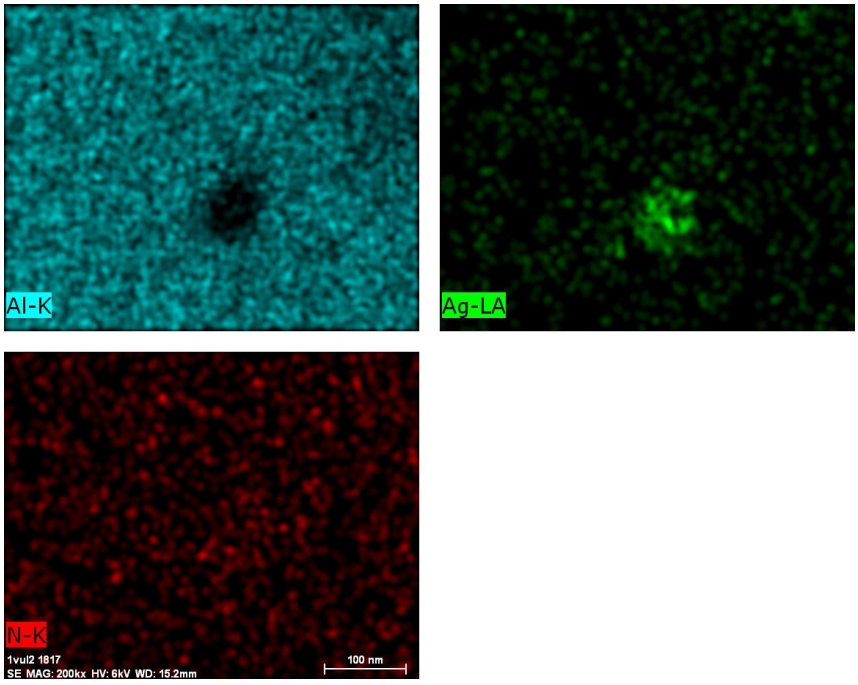

Figure 5-7: EDS analysis results

Aluminum and nitrogen were also detected in specimen in spectroscopy results. Aluminum served the substrate, but the presence of nitrogen indicates that not all of the precursor solution was thermally decomposed into silver nanoparticles; some amount was able to pass unprocessed and dried up on the coated surface.

5.3.2 Variable flame temperature

The lower flame temperatures produced slightly different results. With precursor concentration 300 mg/l and maximum flame temperature at ~780°C, nanoparticle size measured to be between 35nm and 60nm. When precursor concentration was reduced to 100 mg/l, the range of size of particles reduced to be between 26nm and 48nm. For third specimen, the precursor concentration was 100 mg/l and the maximum flame temperature was increased to 830°C. The size of particles increased drastically to about 100 to 115 nm.

Therefore it can be said that the nanoparticles size decreases with decrease in concentration of precursor solution at lower temperatures. However, it increases radically when the flame temperature was increased. These relations for flame spray synthesis of silver nanoparticle agree with the results reported in literature, other than the effect of precursor concentration which Mäkela et al. [111] suggested play no role in nanoparticle size.

5.3.3 One step superhydrophilic coating

Optically transparent coating proved to have superhydrophilic properties. The contact angle measurement of 2 µl water droplet on coated glass surface dropped from 18 degrees to about 9.5 degrees in about 5 seconds and hence the surface showed superhydrophilic characteristic as per definition (see Figure 5-8). Therefore, system's ability to produce functional coating in a single step process has been confirmed.

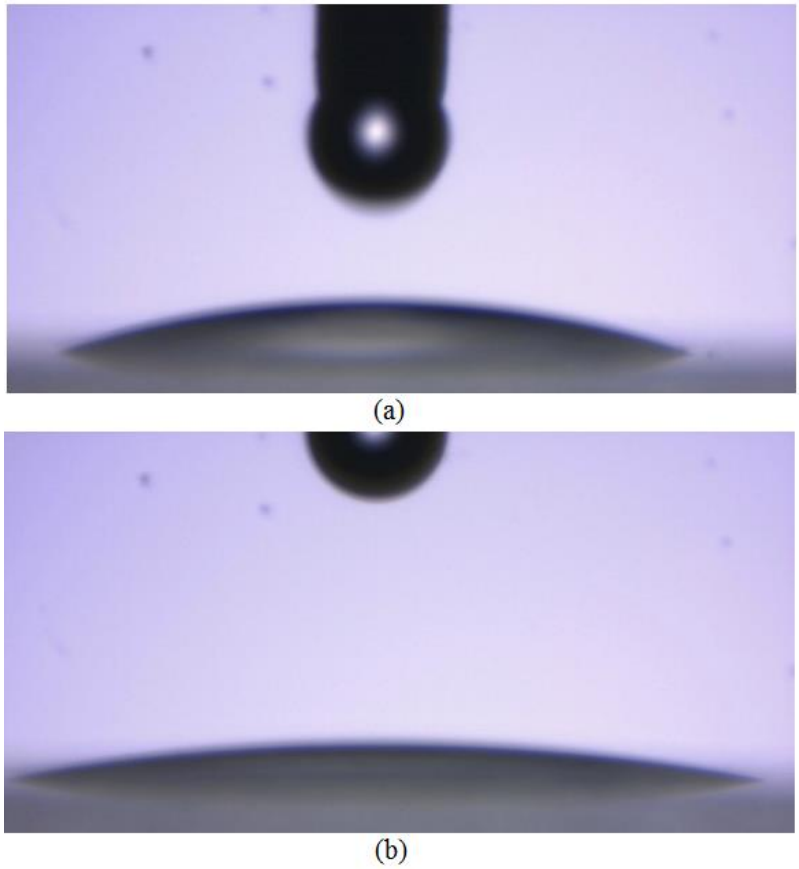

Figure 5-8: Coated microscopic glass slide (a) at 0s (b) after ~5s

5.4 Conclusions

As a result of the preliminary testing of the proposed flame spray pyrolysis technique, silver nanoparticles averaging between 25nm and 40nm in size were successfully synthesized and deposited onto aluminum and glass substrates. The dependence of the synthesized particles size on such parameters as the atomizer frequency and precursor concentration was also studied. Experimental results showed that larger precursor droplets tend to produce smaller particles and, somewhat unexpectedly, smaller precursor concentrations resulted in larger apparent particle sizes. Further experiments were conducted with elevated flame temperature which produced rapid increase in particle sizes which corresponds to the results described in literature. Later sample analysis

revealed traces of precursor material present on coated substrate. The reduction of unwanted precursor residue is a function of fine tuning coating and synthesis parameters such as flame temperature, precursor concentration, feed rate, and the nozzle-substrate distance.

In addition, a functional superhydrophilic coating on glass substrate was also produced. Obtained water contact angles can be further reduced by adjusting the system to create particles of smaller size thus increasing nano-scale roughness possibly creating antifogging effect.

Chapter 6 **Conclusions and future work**

The research work presented in this dissertation is comprised of four papers and provides a description of the evolution of a novel deposition system capable of resolving some of the shortcomings of established spray coating techniques. Furthermore, during the system's development, new nanoparticle generation functionality of the proposed design was also explored.

Key contributions that follow from the work presented are summarized below:

6.1 Dual Velocity Coating System Development and Initial Performance Evaluation

Chapter 2 laid the foundation for the research presented in this dissertation by introducing common problems in spray coating and the ways in which some of them can be resolved. Furthermore, a novel design of a coating system is presented and its performance is tested and analysed for different coating applications. The core principle of the system's operation is the decoupling of the droplet generation device and the nozzle that facilitates close to optimum coating conditions. A dual regime nozzle ensures the particles travel through the nozzle at relatively low velocity to prevent particle adhesion to the interior walls. Simultaneously, at the exit of the nozzle the particles are accelerated to enter the "spreading" regime as outlined in the particle impact dynamics section. The unique tunability and adaptability of the system configuration allows nozzle design changes suitable for a number of different coating applications. The potential of the system to be used in conventional spray coating and micro printing have been demonstrated.

6.2 Utilization of the Updated Coating System for Silver Nanoparticle Coating

In Chapter 3, silver nanoparticles of ~15nm in diameter were successfully synthesized and coated onto a glass substrate. The coating technique involved the use of a dual regime coating apparatus, which allows for fine coating thickness control and layer uniformity. Through precise droplet velocity control, the system facilitates near ideal droplet impact conditions at the surface, minimizing the chance of clogging/condensation inside the nozzle. Furthermore, focusing effect of the nozzle produces much less waste as most droplets are deposited onto the surface having the velocity falling into the "spreading regime" window. The coating produced exhibited strong superhydrophilic properties with water contact angles of around 6 degrees, and is shown to possess antifogging properties. In addition, coated samples showed a slight improvement in light transmission in the visible spectrum with the average increase of approximately 0.7% in dry state and nearly 25% in foggy state. The unique combination of antibacterial properties of silver nanoparticles, together with superhydrophilic and antireflective behavior of the produced coating may potentially benefit numerous areas of research and industry, particularly in the biomedical sector.

6.3 Introduction of a Novel Thermally Assisted Coating Technique

Chapter 4 builds upon the findings reported in previous chapters and introduces a new design feature. The coating system described in this chapter realizes a dual velocity regime to ensure close to optimum conditions both inside the nozzle and at the substrate surface. Additionally, built in ring flame jet allows to heat the particles passing through nozzle's exit. This combination can provide the advantage of single step coating with minimal post processing. In-situ sintering using the ring flame has been demonstrated.

The coating system has been used to coat surfaces with nanoparticles to improve hydrophilic properties of the surface. Further exploration of the capabilities of the system will allow finding new applications and improve system's performance.

6.4 Application of Annular Flame Nozzle Design in Flame Spray Pyrolysis for *in situ* Nanoparticle Generation

In Chapter 5, a novel flame spray pyrolysis method is introduced. As a result of the preliminary testing of the proposed flame spray pyrolysis technique, silver nanoparticles averaging between 25nm and 40nm in size were successfully synthesized and deposited onto aluminum and glass substrates. The dependence of the synthesized particle's size on such parameters as the atomizer frequency and precursor concentration was also studied. Experimental results showed that larger precursor droplets tend to produce smaller particles and, somewhat unexpectedly, smaller precursor concentrations resulted in larger apparent particle sizes. Further experiments were conducted with elevated flame temperature which produced rapid increase in particle sizes which corresponds to the results described in literature. Later sample analysis revealed traces of precursor material present on coated substrate. The reduction of unwanted precursor residue is a function of fine tuning coating and synthesis parameters such as flame temperature, precursor concentration, feed rate, and the nozzle-substrate distance.

In addition, a functional superhydrophilic coating on glass substrate was also produced. Obtained water contact angles can be further reduced by adjusting the system to create particles of smaller size thus increasing nano-scale roughness possibly creating antifogging effect.

6.5 Limitations of current designs

The main limitation of the current system designs presented in this work is their generality. Nozzles were designed and manufactured to illustrate the idea and are not perfectly tuned to a particular application. Current nozzle design is not ideally suited for large area coating and needs to be scaled up as well as incorporate nozzle tips with non-circular shape for better coverage. Micro-printing application requires the nozzle to be scaled down and the change of the central high speed tube to a shape that will better facilitate the flow focusing effect. Pyrolysis setup, although showed promising results, needs to be optimized to provide better thermal control within the space where the thermal decomposition reaction takes place. Also, a separate nozzle should be made for the sole purpose of nanoparticle generation to better facilitate the recovery of generated particles.

6.6 Future work

Future research work that will extend and complement results presented in this dissertation may include the following topics.

The system presented in Chapter 2 and Chapter 3 represents a compromise in terms of size and applications it can be used for. Therefore, based on the same principles outlined in these chapters, a system for a large area coating can also be developed. The system can be utilized for deposition of various materials on surfaces such as glass windows, photovoltaic panels, automotive applications, etcetera. Optimization of the system may include experiments and development nozzle shapes that will better facilitate coating of large samples with minimal movement and better coverage of the area. The system's optimization may also proceed in a complete opposite direction.

Early experiments in microprinting/coating have shown the system's ability to be miniaturized producing printed lines as narrow as 50μm. The first experiments in microprinting were performed with the basic system design that did not include the flow conditioning unit and did not have the concentric geometry characteristic to the later design. Downscaling a nozzle with updated geometry will most likely allow to significantly reduce the minimal width of a printed feature while making it more consistent at the same time.

Since the main focus of the presented research was on development of the system itself, only limited amount of work was done on determining the suitability of the nozzle for various applications. Furthermore, the research effort concentrated on various materials used for coating in conjunction with their interaction with the coating device and substrate can also be explored. One important property of the final deposited layer that depends on coating and base material as well as on the method of application is the adhesion to the substrate. This topic have been widely researched and the proposed system's improvements with respect to the coating adhesion may complement research previously completed.

Pyrolysis technique introduced in this dissertation allows for fine tuning of process parameters. Experimental conditions such as temperature, droplet diameter, droplet residence time, etc. have been roughly established for silver nanoparticle synthesis and can be further refined to achieve predictable results. Furthermore, a wide range of materials can be produced using the technique, and device described in this dissertation provide a useful tool for future research in material processing in general and nanoparticle production in particular.

Finally, all of the devices and techniques presented in this dissertation depend on a reliable atomization device that can consistently produce droplets of a particular size consistently. Moreover, this device should be able to process a range of materials used in coatings including various solvents and precursor solutions (in case of pyrolysis). Ultrasonic nebulisers used in most of the experiments presented in this dissertation provide somewhat consistent performance. However, performance of these nebulizers is strongly dependant on liquid properties such as viscosity, temperature, and density. Therefore, the range of materials that can be processed is limited. Development of an atomizing device that can accommodate a wider range of materials while providing stable and consistent performance will complement coating system introduced in this dissertation.

Bibliography

1. Böttger, P.H.M., et al., *Hard wear-resistant coatings with anisotropic thermal conductivity for high thermal load applications.* Journal of Applied Physics, 2014. **116**(1): p. 013507.

2. Janković, A., et al., *Graphene-based antibacterial composite coatings electrodeposited on titanium for biomedical applications.* Progress in Organic Coatings, 2015. **83**: p. 1-10.

3. Krebs, F.C., *Fabrication and processing of polymer solar cells: A review of printing and coating techniques.* Solar Energy Materials & Solar Cells, 2009. **93**(4): p. 394-412.

4. Lien, D.-H., et al., *All-Printed Paper Memory.* ACS Nano, 2014. **8**(8): p. 7613-7619.

5. Van de Groep, J., P. Spinelli, and A. Polman, *Single-Step Soft-Imprinted Large-Area Nanopatterned Antireflection Coating.* Nano Letters, 2015. **15**(6): p. 4223-4228.

6. Wu, L., X. Guo, and J. Zhang, *Abrasive Resistant Coatings—A Review.* Lubricants, 2014. **2**(2): p. 66.

7. Birnie, D.P., *Spin Coating Technique*, in *Sol-Gel Technologies for Glass Producers and Users*, M.A. Aegerter and M. Mennig, Editors. 2004, Springer US: Boston, MA. p. 49-55.

8. Kamaruddin, S.A., et al., *Zinc oxide films prepared by sol–gel spin coating technique.* Applied Physics A, 2011. **104**(1): p. 263-268.

9. Goebbert, C., et al., *Wet chemical deposition of ATO and ITO coatings using crystalline nanoparticles redispersable in solutions.* Thin Solid Films, 1999. **351**(1): p. 79-84.

10. Negishi, N., K. Takeuchi, and T. Ibusuki, *Preparation of the TiO2 Thin Film Photocatalyst by the Dip-Coating Process.* Journal of Sol-Gel Science and Technology, 1998. **13**(1): p. 691-694.

11. Jensen, K.F., *Chemical Vapor Deposition*, in *Microelectronics Processing*1989, American Chemical Society. p. 199-263.

12. Archer, N.J., *Chemical vapour deposition.* Physics in Technology, 1979. **10**(4): p. 152.

13. Boone, D.H., *Physical vapour deposition processes.* Materials Science and Technology, 1986. **2**(3): p. 220-224.

14. Weiss, K., et al., *Development of different copper seed layers with respect to the copper electroplating process.* Microelectronic Engineering, 2000. **50**(1): p. 433-440.

15. Mizushima, I., et al., *Development of a new electroplating process for Ni–W alloy deposits.* Electrochimica Acta, 2005. **51**(5): p. 888-896.

16. Bladon, J.J., *Pretreatment for electroplating process*, 1990, Google Patents.

17. Tsangaraki-Kaplanoglou, I., et al., *Effect of alloy types on the anodizing process of aluminum.* Surface and Coatings Technology, 2006. **200**(8): p. 2634-2641.

18. Surganov, V. and A. Mozalev, *Planar aluminum interconnection formed by electrochemical anodizing technique.* Microelectronic Engineering, 1997. **37**: p. 329-334.

19. De Groot, K., et al., *Plasma sprayed coatings of hydroxylapatite.* Journal of Biomedical Materials Research, 1987. **21**(12): p. 1375-1381.

20. Muehlberger, E. and R.D. Kremith, *System and method for plasma coating*, 1982, Google Patents.

21. Banerjee, A., P. Nath, and H.C. Ovshinsky, *Method for plasma - coating a semiconductor body*, 1988, Google Patents.

22. Jun, M.B., et al., *An Experimental Evaluation of an Atomization-Based Cutting Fluid Application System for Micromachining.* Journal of Manufacturing Science and Engineering, 2008. **130**(3): p. 031118-031118-8.

23. Rukosuyev, M., et al., *Design and Development of Cutting Fluid System Based on Ultrasonic Atomization for Micro-Machining.* SME Technical Paper : TP. Vol. 38. 2010, Dearborn, Mich.: Society of Manufacturing Engineers.

24. Rukosuyev, M., C.S. Goo, and M.B.G. Jun, *Understanding the effects of the system parameters of an ultrasonic cutting fluid application system for micro-machining.* Journal of Manufacturing Processes, 2010. **12**(2): p. 92-98.

25. Bourgeat-Lami, E. and J. Lang, *Encapsulation of Inorganic Particles by Dispersion Polymerization in Polar Media: 1. Silica Nanoparticles Encapsulated by Polystyrene.* Journal of Colloid and Interface Science, 1998. **197**(2): p. 293-308.

26. Yao, J., et al., *Thermal barrier coating bonded by (Al2O3–Y2O3)/(Y2O3-stabilized ZrO2) laminated composite coating prepared by two-step cyclic spray pyrolysis.* Corrosion Science, 2014. **80**: p. 37-45.

27. Rukosuyev, M.V., et al., *Design and application of nanoparticle coating system with decoupled spray generation and deposition control.* Journal of Coatings Technology and Research, 2016. **13**(5): p. 769-779.

28. Rukosuyev, M., et al., *Uniform silver nanoparticles coating using dual regime spray deposition system for superhydrophilic and antifogging applications.* Journal of Coatings Technology and Research, 2017. **14**(2): p. 347-354.

29. Rukosuyev, M., S. Baqar, and M. Jun, *Development and Evaluation of Flame Assisted Dual Velocity Nanoparticle Coating System.* Journal of Micro and Nano-Manufacturing, 2017.

30. Ha, D., et al., *Paper-Based Anti-Reflection Coatings for Photovoltaics.* Advanced Energy Materials, 2014. **4**(9): p. n/a-n/a.

31. Krebs, F.C., *Fabrication and processing of polymer solar cells: A review of printing and coating techniques.* Solar Energy Materials and Solar Cells, 2009. **93**(4): p. 394-412.

32. Mundo, C., M. Sommerfeld, and C. Tropea, *Droplet-wall collisions: Experimental studies of the deformation and breakup process.* International Journal of Multiphase Flow, 1995. **21**(2): p. 151-173.

33. Othman, S.H., et al., *Dispersion and stabilization of photocatalytic TiO2 nanoparticles in aqueous suspension for coatings applications.* J. Nanomaterials, 2012. **2012**: p. 2-2.

34. Scher, H.B., et al., *Aerosol coating process based on volatile, non-flammable solvents*, 2015, Google Patents.

35. Kramer, I.J., et al., *Efficient Spray-Coated Colloidal Quantum Dot Solar Cells.* Advanced Materials, 2015. **27**(1): p. 116-121.

36. Byun, D.Y., V.D. Nguyen, and B.H. Seong, *Coating System Using Spray Nozzle*, 2015, Google Patents.

37. Simon, J.C., et al., *Ultrasonic atomization of liquids in drop-chain acoustic fountains.* Journal of Fluid Mechanics, 2015. **766**.

38. Lang, R.J., *Ultrasonic atomization of liquids.* Acoustical Society of America -- Journal, 1962. **34**(1): p. 6-8.

39. Wood, R.W. and A.L. Loomis, *The Physical and Biological Effects of High-Frequency Sound Waves of Great Intensity.* Phil. Mag., 1927. **4**: p. 417-136.

40. Avvaru, B., et al., *Ultrasonic atomization: Effect of liquid phase properties.* Ultrasonics, 2006. **44**(2): p. 146-158.

41. Stow, C.D. and M.G. Hadfield, *An Experimental Investigation of Fluid Flow Resulting from the Impact of a Water Drop with an Unyielding Dry Surface.* Proceedings of the Royal Society of London A: Mathematical, Physical and Engineering Sciences, 1981. **373**(1755): p. 419-441.

42. Jun, M.B.G., et al., *An experimental evaluation of an atomization-based cutting fluid application system for micromachining.* Journal of Manufacturing Science and Engineering, 2008. **130**(3): p. 031118-1.

43. Dongjo, K., J. Sunho, and M. Jooho, *Synthesis of silver nanoparticles using the polyol process and the influence of precursor injection.* Nanotechnology, 2006. **17**(16): p. 4019.

44. Tettey, K.E., M.I. Dafinone, and D. Lee, *Progress in Superhydrophilic Surface Development.* MATERIALS EXPRESS. **1**(2): p. 89-104.

45. Zhang, J.L. and S.J. Severtson, *Fabrication and use of artificial superhydrophilic surfaces.* JOURNAL OF ADHESION SCIENCE AND TECHNOLOGY. **28**(8-9): p. 751-768.

46. Funakoshi, K. and T. Nonami, *Photocatalytic treatments on dental mirror surfaces using hydrolysis of titanium alkoxide.* Journal of Coatings Technology and Research, 2007. **4**(3): p. 327-333.

47. Ohdaira, T., et al., *Antifogging effects of a socket-type device with the superhydrophilic, titanium dioxideâ€“coated glass for the laparoscope.* Surgical Endoscopy, 2007. **21**(2): p. 333-338.

48. Huang, C.-J., et al., *Bioinspired Zwitterionic Surface Coatings with Robust Photostability and Fouling Resistance.* ACS Applied Materials & Interfaces, 2015. **7**(42): p. 23776-23786.

49. Shivapooja, P., et al., *Modification of Silicone Elastomer Surfaces with Zwitterionic Polymers: Short-Term Fouling Resistance and Triggered Biofouling Release.* ACS Applied Materials & Interfaces, 2015. **7**(46): p. 25586-25591.

50. Guangxu, C., et al., *A Novel Way to Fabricate Superhydrophilic and Antibacterial TiO 2 Nanofilms on Glass by Ion Implantation and Subsequent Annealing.* Japanese Journal of Applied Physics, 2013. **52**(10R): p. 100207.

51. Chun, Y., et al., *Superhydrophilic surface treatment for thin film NiTi vascular applications.* Materials Science and Engineering: C, 2009. **29**(8): p. 2436-2441.

52. Tugulu, S., et al., *Preparation of superhydrophilic microrough titanium implant surfaces by alkali treatment.* Journal of Materials Science: Materials in Medicine. **21**(10): p. 2751-2763.

53. Fujishima, A., X. Zhang, and D.A. Tryk, *TiO2 photocatalysis and related surface phenomena.* Surface Science Reports, 2008. **63**(12): p. 515-582.

54. Xu, L., et al., *Reversible conversion of conducting polymer films from superhydrophobic to superhydrophilic.* Angewandte Chemie (International ed.), 2005. **44**(37): p. 6009-6012.

55. Zhang, J., et al., *Reversible Superhydrophobicity to Superhydrophilicity Transition by Extending and Unloading an Elastic Polyamide Film.* Macromolecular Rapid Communications, 2005. **26**(6): p. 477-480.

56. Jiang, Y., et al., *Self-Assembled Monolayers of Dendron Thiols for Electrodeposition of Gold Nanostructures:Toward Fabrication of Superhydrophobic/Superhydrophilic Surfaces and pH-Responsive Surfaces.* Langmuir, 2005. **21**(5): p. 1986-1990.

57. Sun, T.L., et al., *Reversible switching between superhydrophilicity and superhydrophobicity.* ANGEWANDTE CHEMIE-INTERNATIONAL EDITION, 2004. **43**(3): p. 357-360.

58. Dong, W., et al., *Investigation on the Antibacterial Micro-Porous Titanium with Silver Nano-Particles.* JOURNAL OF NANOSCIENCE AND NANOTECHNOLOGY. **13**(10): p. 6782-6786.

59. Prasad, M.H., D. Kalpana, and N.J. Kumar, *Silver Nano Coating on Glass Substrate and Antibacterial Activity of Silver Nano particles Synthesised by Arachis hypogaea L. Leaf Extract.* CURRENT NANOSCIENCE. **8**(2): p. 280-285.

60. Sarkar, S., et al., *Facile synthesis of silver nano particles with highly efficient anti-microbial property.* Polyhedron, 2007. **26**(15): p. 4419-4426.

61. Kim, K.-J., et al., *Antifungal activity and mode of action of silver nano-particles on Candida albicans.* BioMetals, 2009. **22**(2): p. 235-242.

62. Chladek, G., et al., *Antifungal Activity of Denture Soft Lining Material Modified by Silver Nanoparticles-A Pilot Study.* INTERNATIONAL JOURNAL OF MOLECULAR SCIENCES. **12**(7): p. 4735-4744.

63. Rai, M., et al., *Broad-spectrum bioactivities of silver nanoparticles: the emerging trends and future prospects.* Applied Microbiology and Biotechnology. **98**(5): p. 1951-1961.

64. Lesina, A.C., et al., *Modeling and Characterization of Antireflection Coatings with Embedded Silver Nanoparticles for Silicon Solar Cells.* Plasmonics. **10**(6): p. 1525-1536.

65. Nishioka, K., T. Sueto, and N. Saito, *Formation of antireflection nanostructure for silicon solar cells using catalysis of single nano-sized silver particle.* Applied Surface Science, 2009. **255**(23): p. 9504-9507.

66. Sun, Y. and Y. Xia, *Shape-Controlled Synthesis of Gold and Silver Nanoparticles.* Science, 2002. **298**(5601): p. 2176-2179.

67. Donati, I., et al., *Polyol Synthesis of Silver Nanoparticles: Mechanism of Reduction by Alditol Bearing Polysaccharides.* Biomacromolecules, 2009. **10**(2): p. 210-213.

68. Khanlary, M.R. and E. Salavati, *Optical Properties and Characterization of Prepared Sn-Doped PbSe Thin Film.* Advances in Condensed Matter Physics, 2012. **2012**: p. 4.

69. Simon, J.C., et al., *Ultrasonic atomization of liquids in drop-chain acoustic fountains.* Journal of Fluid Mechanics, 2015. **766**: p. 129-146.

70. Nelson, G.M., J.A. Nychka, and A.G. McDonald, *Flame Spray Deposition of Titanium Alloy-Bioactive Glass Composite Coatings.* Journal of Thermal Spray Technology, 2011. **20**(6): p. 1339-1351.

71. Sainz, M.A., M.I. Osendi, and P. Miranzo, *Protective Si–Al–O–Y glass coatings on stainless steel in situ prepared by combustion flame spraying.* Surface and Coatings Technology, 2008. **202**(9): p. 1712-1717.

72. Bartuli, C., T. Valente, and M. Tului, *Plasma spray deposition and high temperature characterization of ZrB2–SiC protective coatings.* Surface and Coatings Technology, 2002. **155**(2–3): p. 260-273.

73. Ermakov, S.S. and A.M. Shmakov, *Flame-spray deposition of coatings on sintered materials. Part 1.* Soviet Powder Metallurgy and Metal Ceramics, 1986. **25**(3): p. 191-194.

74. Song, J., et al., *Flame treatment of low-density polyethylene: Surface chemistry across the length scales.* Applied Surface Science, 2007. **253**(24): p. 9489-9499.

75. Bayer, I.S., A.J. Davis, and A. Biswas, *Robust superhydrophobic surfaces from small diffusion flame treatment of hydrophobic polymers.* RSC Advances, 2014. **4**(1): p. 264-268.

76. Bayer, I.S., A. Steele, and E. Loth, *Superhydrophobic and electroconductive carbon nanotube-fluorinated acrylic copolymer nanocomposites from emulsions.* Chemical Engineering Journal, 2013. **221**: p. 522-530.

77. Naha, S., S. Sen, and I.K. Puri, *Flame synthesis of superhydrophobic amorphous carbon surfaces.* Carbon, 2007. **45**(8): p. 1702-1706.

78. Gadow, R., A. Killinger, and J. Rauch, *Introduction to High-Velocity Suspension Flame Spraying (HVSFS).* Journal of Thermal Spray Technology, 2008. **17**(5): p. 655-661.

79. Poirier, T., et al., *Deposition of nanoparticle suspensions by aerosol flame spraying: Model of the spray and impact processes.* Journal of Thermal Spray Technology, 2003. **12**(3): p. 393-402.

80. Karthikeyan, J., et al., *Nanomaterial powders and deposits prepared by flame spray processing of liquid precursors.* Nanostructured Materials, 1997. **8**(1): p. 61-74.

81. Madler, L., et al., *Direct formation of highly porous gas-sensing films by in situ thermophoretic deposition of flame-made Pt/SnO2 nanoparticles.* SENSORS AND ACTUATORS B-CHEMICAL, 2006. **114**(1): p. 283-295.

82. Teisala, H., et al., *Development of superhydrophobic coating on paperboard surface using the Liquid Flame Spray.* Surface and Coatings Technology. **205**(2): p. 436-445.

83. Strobel, R., A. Alfons, and S.E. Pratsinis, *Aerosol flame synthesis of catalysts.* Advanced Powder Technology, 2006. **17**(5): p. 457-480.

84. Rosner, D.E., *Flame Synthesis of Valuable Nanoparticles:â€‰ Recent Progress/Current Needs in Areas of Rate Laws, Population Dynamics, and Characterization.* Industrial & Engineering Chemistry Research, 2005. **44**(16): p. 6045-6055.

85. Teoh, W.Y., R. Amal, and L. MÃ¤dler, *Flame spray pyrolysis: An enabling technology for nanoparticles design and fabrication.* NANOSCALE. **2**(8): p. 1324-1347.

86. Purwanto, A., H. Widiyandari, and A. Jumari, *Fabrication of high-performance fluorine dopedâ€“tin oxide film using flame-assisted spray deposition.* Thin Solid Films. **520**(6): p. 2092-2095.

87. Mädler, L., W.J. Stark, and S.E. Pratsinis, *Flame-made Ceria Nanoparticles.* Journal of Materials Research, 2002. **17**(06): p. 1356-1362.

88. Perednis, D. and L.J. Gauckler, *Thin Film Deposition Using Spray Pyrolysis.* Journal of Electroceramics, 2005. **14**(2): p. 103-111.

89. Hansen, J.P., et al., *Synthesis of ZnO particles in a quench-cooled flame reactor.* AIChE Journal, 2001. **47**(11): p. 2413-2418.

90. MÃ¤dler, L., et al., *Controlled synthesis of nanostructured particles by flame spray pyrolysis.* Journal of Aerosol Science, 2002. **33**(2): p. 369-389.

91. Johannessen, T., et al., *Product Design and EngineeringFlame Synthesis of Nanoparticles.* Chemical Engineering Research and Design, 2004. **82**(11): p. 1444-1452.

92. Pratsinis, S.E., W. Zhu, and S. Vemury, *The role of gas mixing in flame synthesis of titania powders.* Powder Technology, 1996. **86**(1): p. 87-93.

93. Jensen, J.R., et al., *A study of Cu/ZnO/Al2O3 methanol catalysts prepared byÂ flameÂ combustion synthesis.* Journal of Catalysis, 2003. **218**(1): p. 67-77.

94. Mädler, L., et al., *Controlled synthesis of nanostructured particles by flame spray pyrolysis.* Journal of Aerosol Science, 2002. **33**(2): p. 369-389.

95. MÃ¤kelÃ¤, J.M., et al., *Nanoparticle Deposition from Liquid Flame Spray onto Moving Roll-to-Roll Paperboard Material.* Aerosol Science and Technology. **45**(7): p. 827-837.

96. Kammler, H.K., L. Mädler, and S.E. Pratsinis, *Flame Synthesis of Nanoparticles.* Chemical Engineering & Technology, 2001. **24**(6): p. 583-596.

97. Pratsinis, S.E., *Aerosol-based technologies in nanoscale manufacturing: from functional materials to devices through core chemical engineering.* AIChE Journal. **56**(12): p. 3028-3035.

98. Tricoli, A. and T.D. Elmøe, *Flame spray pyrolysis synthesis and aerosol deposition of nanoparticle films.* AIChE Journal. **58**(11): p. 3578-3588.

99. Cho, K., et al., *Mechanisms of the Formation of Silica Particles from Precursors with Different Volatilities by Flame Spray Pyrolysis.* Aerosol Science and Technology, 2009. **43**(9): p. 911-920.

100. Makela, J.M., et al., *Collection of liquid flame spray generated TiO2 nanoparticles on stainless steel surface.* Materials Letters, 2006. **60**(4): p. 530-534.

101. Aromaa, M., H. Keskinen, and J.M. MÃ¤kelÃ¤, *The effect of process parameters on the Liquid Flame Spray generated titania nanoparticles.* Biomolecular Engineering, 2007. **24**(5): p. 543-548.

102. Guild, C., et al., *Perspectives of spray pyrolysis for facile synthesis of catalysts and thin films: An introduction and summary of recent directions.* Catalysis Today. **238**: p. 87-94.

103. Pimenoff, J.A., A.K. Hovinen, and M.J. Rajala, *Nanostructured coatings by liquid flame spraying.* Thin Solid Films, 2009. **517**(10): p. 3057-3060.

104. Pratsinis, S.E., *Flame aerosol synthesis of ceramic powders.* Progress in Energy and Combustion Science, 1998. **24**(3): p. 197-219.

105. You, H., et al., *Synthesis of yttria-stabilized zirconia film by Aerosol Flame Pyrolysis Deposition.* Journal of Analytical and Applied Pyrolysis, 2008. **81**(1): p. 14-19.

106. Mäkelä, J.M., et al., *Collection of liquid flame spray generated TiO2 nanoparticles on stainless steel surface.* Materials Letters, 2006. **60**(4): p. 530-534.

107. Mueller, R., L. MÃ¤dler, and S.E. Pratsinis, *Nanoparticle synthesis at high production rates by flame spray pyrolysis.* Chemical Engineering Science, 2003. **58**(10): p. 1969-1976.

108. Tikkanen, J., et al., *Characteristics of the liquid flame spray process.* Surface and Coatings Technology, 1997. **90**(3): p. 210-216.

109. Pluym, T.C., et al., *Aerosols in Materials Processing Solid silver particle production by spray pyrolysis.* Journal of Aerosol Science, 1993. **24**(3): p. 383-392.

110. Pingali, K.C., D.A. Rockstraw, and S. Deng, *Silver Nanoparticles from Ultrasonic Spray Pyrolysis of Aqueous Silver Nitrate.* Aerosol Science and Technology, 2005. **39**(10): p. 1010-1014.

111. Mäkelä, J.M., et al., *Generation of metal and metal oxide nanoparticles by liquid flame spray process.* Journal of Materials Science, 2004. **39**(8): p. 2783-2788.

112. Rukosuyev, M.V., et al., *Design and application of nanoparticle coating system with decoupled spray generation and deposition control.* Journal of Coatings Technology and Research: 2016. **13**(5): p. 769-779.